NASA

Technical Memorandum 80276

A Three-Dimensional Model of Corotating Streams in the Solar Wind II. Hydrodynamic Streams

Victor J. Pizzo

April 1979

National Aeronautics and Space Administration

Goddard Space Flight Center
Greenbelt, Maryland 20771

A THREE-DIMENSIONAL MODEL OF COROTATING STREAMS IN THE SOLAR WIND

II. HYDRODYNAMIC STREAMS

by

Victor J. Pizzo*
NASA/Goddard Space Flight Center
Laboratory for Extraterrestrial Physics
Greenbelt, MD 20771

TO BE SUBMITTED TO: The Journal of Geophysical Research

*NAS/NRC Resident Research Associate

ABSTRACT

This paper explores theoretical aspects of corotating solar wind dynamics on a global scale by means of numerical simulations executed with a nonlinear, inviscid, adiabatic, single-fluid, three-dimensional (3-D) hydrodynamic formulation. The study begins with a simple, hypothetical 3-D stream structure defined on a source surface located at 35 R_S and carefully documents its evolution to 1 AU under the influence of solar rotation. By manipulating the structure of this prototype configuration at the source surface, it is possible to elucidate the factors most strongly affecting stream evolution: 1) the intrinsic correlations among density, temperature, and velocity existing near the source; 2) the amplitude of the stream; 3) the longitudinal breadth of the stream; 4) the latitudinal breadth of the stream; and 5) the heliographic latitude of the centroid of the stream. The action of these factors is best understood in terms of momentum arguments of relative simplicity and general application (to the extent that waves, conduction, and kinetic effects may be ignored). Corotating structure is viewed as a spiral standing wave (in the rotating frame) in which there is an ongoing competition between the kinematic tendency of the stream to steepen (as high-speed material overtakes slow) and the dynamical reaction of the gas to resist compression (through acceleration and tangential deflection of material by pressure gradients in the interaction region). Longitudinal gradients in the radial velocity distribution determine how fast material is brought into the interaction region, but the detailed momentum balance as a function of position within the stream dictates what happens when the material collides. Reasonable specifications of the five factors mentioned above can so affect this kinematic-dynamic balance that even a high-amplitude stream (e.g., peak-to-trough velocity differences at 1 AU $\simeq$ 480 km/s) may be prevented from shocking inside 1 AU, where the nonradial-flow broadening mechanism operates most efficiently. The nonlinear 3-D capabilities of the model allow quantitative study of the global development of this induced tangential flow in some detail. The nonradial motions lead to the net latitudinal transport of small amounts (a few percent) of mass, energy, and momentum. The effects of the latitudinal transport upon the evolution

within an east-west plane are minimal, and the latitudinal spreading of stream material in interplanetary space, even in the presence of steep meridional gradients (up to 30 km/s/deg), is limited to a few degrees. Thus, for corotating structures, with their favorable spiral geometry, the 2-D approximation adequately describes the dynamical interaction. However, certain important research topics can only be approached in the full 3-D formulation. For example, the systematic pattern of the meridional flow changes across stream fronts contain information on the 3-D structure of the stream and thus offers promise as a practical diagnostic tool. Also, since the magnetic field is tied to the flow, it is to be expected that stream-driven meridional motions should have a noticeable effect upon the north-south magnetic fluctuations and may be of consequence to angular momentum studies. Proper discussion of these subjects demands a 3-D MHD model and will be considered in a subsequent paper.

INTRODUCTION

The solar corona exhibits an organized, large-scale, three-dimensional (3-D) structure that can remain relatively stable over periods of several rotations (for recent reviews, see Hundhausen, 1977; Zirker, 1977). Since the corona is the source of the solar wind, it is natural to question how this structure evolves as it propagates into interplanetary space and sweeps past the earth into the far reaches of the solar system. Observationally, we have been laboring under a severe handicap, as spacecraft measurements are restricted to a narrow band of latitudes about the solar equatorial plane. Thus, the vast bulk of the solar wind has never been directly examined. Instead, in our efforts to achieve a global perspective on the solar wind expansion, we have been forced to rely on marginal statistical inferences drawn from single and infrequent multiple spacecraft observations, supplemented by somewhat less precise though more inclusive measurements obtained by interplanetary scintillation and radio-scattering techniques (Hewish, 1972; Woo, 1975). Therefore, until the advent of the Out-of-the-Ecliptic (Solar-Polar) Mission, further insights into the mechanics of the global solar wind flow must be wrested primarily from theoretical studies.

Models of the inhomogeneous, supersonic, corotating solar wind have attained a high level of sophistication. Under the continuum fluids description, such features as nonlinearities, two and three-dimensional geometries, separate treatment of protons and electrons, and the smooth interplanetary magnetic field have been incorporated in various approaches (e.g., Carovillano and Siscoe, 1969; Goldstein, 1971; Siscoe and Finley, 1972; Matsuda and Sakurai, 1972; Hundhausen, 1973a; Nakagawa and Wellck, 1973; Dryer and Steinolfson, 1976; Barouch and Burlaga, 1976; Goldstein and Jokipii, 1977; Han, 1977; and Riesebieter, 1977). We can now justifiably anticipate that the application of such models in a comprehensive theoretical investigation should lead to valuable insights into the nature of the global solar wind flow. Even in the absence of suitable observations, such studies are useful in that they clearly define the limits of current theory and constitute a logical basis for the subsequent analysis and interpretation of empirical data.

This paper is the second in a series of three aimed at providing a general theoretical overview of the interplanetary evolution of global, corotating, solar wind structure. Paper I (Pizzo, 1978) saw the development of a single-fluid, polytropic, inviscid, nonlinear, 3-D hydrodynamic (HD) model which approximates the flow dynamics outside the sonic critical point ($r \gtrsim 35\ R_S$). In this study (II), we apply the model to a broad parameter range of hypothetical HD streams to elucidate the action of the main factors affecting stream evolution in the inner solar system ($r \lesssim 1$ AU). Paper III (Pizzo, 1979) will complete the triad with the presentation of a fully nonlinear 3-D magnetohydrodynamic (MHD) model which will clarify the role of the smooth spiral magnetic field in stream dynamics.

As mentioned above, the literature is replete with model calculations embracing a broad range of physical processes falling under the general category of (magneto-) fluid formulations. In light of this diversity and owing to the intrinsic complexity of multi-dimensional mechanics, one of the chief goals of this paper is to develop some simplified criteria for evaluating the dynamic attributes of any given corotating structure. We will demonstrate that consideration of the distribution of momentum and its partition among its various forms leads to just such a classification scheme. Indeed, it is envisioned as a powerful unifying concept in the analysis of stream models, and, by extension, of spacecraft observations of large-scale interplanetary phenomena.

Within the HD formulation, there exist but a limited number of readily identifiable factors that influence stream evolution. A major portion of this paper is therefore devoted to an extensive computational survey illustrating how these independent factors contribute to stream behavior. While some elements of this study have appeared in the works cited above, an important objective of this paper is to introduce the fundamental aspects of stream dynamics in a systematic, comprehensive way. It is in the presentation of these results that the utility of the momentum arguments shall become apparent.

The nonlinear 3-D properties of this model permit quantitative study of intrinsically global phenomena. For the first time, we are able to obtain reliable estimates of the meridional flow effects attributable to stream interactions and thereby assess the validity of the 2-D and axisymmetric

flow approximations. More importantly, we show that the systematic pattern of north-south motions associated with stream fronts appears to be the only direct manifestation of the parent 3-D structure and, as such, holds promise as a valuable diagnostic tool in probing the unseen reaches of the solar wind away from the ecliptic plane. Furthermore, we discuss the possibility that the meridional flows may have significant impact on angular momentum transport in the solar wind.

This paper is divided into four main sections. First, we briefly review the essential features of the model developed in Paper I. Second, we outline the fundamental issues motivating our selection of examples. Third, we present our computational results, and finally, we discuss the implications of this work from both theoretical and observational standpoints.

THE MODEL

Paper I documents the fundamental mathematical and numerical techniques required to describe the dynamical evolution of 3-D corotating solar wind structure. This numerical model limits attention to those structures that are steady or nearly steady in the frame rotating with the sun and utilizes the single-fluid, polytropic, nonlinear, 3-D HD equations to approximate the dynamics that occur in interplanetary space ($r \gtrsim 35\ R_s$), where the flow is everywhere supersonic and the governing equations hyperbolic. In the inertial frame, the equations are

$$-\Omega \frac{\partial \rho}{\partial \phi} + \nabla \cdot \rho \vec{u} = 0 \tag{1}$$

$$-\Omega \frac{\partial \vec{u}}{\partial \phi} + (\vec{u} \cdot \nabla)\vec{u} = -\frac{1}{\rho} \nabla P - \frac{GM_S}{r^2} \hat{r} \tag{2}$$

$$\left(-\Omega \frac{\partial}{\partial \phi} + \vec{u} \cdot \nabla \right) P\rho^{-\gamma} = 0 \tag{3}$$

where ρ is the mass density (we shall use n, the number density, almost interchangeably), $\vec{u}$ the center of mass velocity, P the total isotropic

(scalar) gas pressure, G the gravitational constant, M_S the solar mass, γ the polytropic index (here = 5/3), and Ω the equatorial angular rotation rate of the sun. The independent variables are the spherical polar coordinates (r,θ,ϕ). The single-fluid temperature, T, is related to the pressure as $P = 2\rho kT/m_p$, where k is Boltzmann's constant and m_p is the proton mass. Conduction, wave dissipation, differential rotation, the magnetic field, and shock heating are all neglected, though the latter two may be incorporated into the model with modest effort. Integration of the finite-difference representation of these equations is performed with the explicit Eulerian method of MacCormack (1971). (For further details, see Paper I.)

METHODOLOGY

Equations (1)-(3) define the physics permitted to the system. While these expressions account for most of the large-scale processes thought important in stream dynamics (see Paper I), the equations themselves are only part of the story, for they encompass several competing physical mechanisms whose precise relationships depend upon the details of the flow conditions imposed near the sun. Foremost among these mechanisms (and the one normally emphasized in discussions of corotating structure) is the rotational alignment process, whereby inhomogeneities in radial expansion speed couple with solar rotation to set up the familiar spiral interaction pattern in interplanetary space (e.g., see Paper I). The mathematical representation of this mechanism is contained on the left-hand side of equations (1)-(3) in the operator

$$-\Omega \frac{\partial}{\partial \phi} + u_r \frac{\partial}{\partial r}.$$

Applied to the radial momentum equation, this isolated portion of the expressions embodies what this paper shall refer to as the kinematic limit, i.e., each fluid element proceeding at constant velocity (c.f. the purely kinematic models of Matsuda and Sakurai, 1972; Barouch and Burlaga, 1976). The pressure force and divergence terms in (1)-(3), on the other hand, describe diffusive dynamical processes which generally oppose the kinematic rotational effects. That is, the interaction between fast and slow flows produces pressure gradients, which in turn induce secondary flows that

relieve the compressional stresses. We shall refer to these pressure-force reactions as the dynamic element in stream evolution.

It is advantageous to visualize the corotating structure as a standing wave (in the rotating frame) having a spiral geometry. This standing wave has two main properties: spatial gradients in radial speed, which determine how fast the interaction proceeds (the kinematic element); and spatial inhomogeneities in the momentum balance, which determine just what happens when the interaction takes place (the dynamic element). We further draw an explicit distinction between the spatial distribution of momentum flux density and the partition of that flux density among kinetic, thermal and magnetic (in the MHD case) forms. The spatial distribution relates to the amount of dynamic inertia conveyed by each fluid element and dictates how much fluid deflection results from the interaction. The partition relates to the speed with which pressure disturbances propagate through the fluid and determines how much of the fluid (i.e., what volume) is affected by the interaction.

In the 3-D solar wind, it is the global distribution of mass, energy, and momentum flux at the source surface that ultimately determines the evolutionary outcome of the competition between the kinematic and dynamic properties of the corotating structure. ('Source surface' pertains to a hypothetical sphere that is centered on the sun and whose radius, r_o, is sufficient to guarantee that the entire surface lies well outside the usual solar wind critical points. Since the equations are hyperbolic, the distribution of variables on this surface are properly called 'initial conditions', but we relax the terminology and equivalently refer to 'boundary' or 'input' or 'source' conditions.) The 3-D distribution at the source surface is dictated by the underlying coronal expansion, which is, as yet, only poorly understood. This lack of complete, detailed knowledge of source conditions does impose the constraint that it may not always be possible to distinguish between a faulty physical description (i.e., the equations) and unrepresentative or overly simplified source conditions. However, as long as we have some idea of the appropriate parameter space, we can reasonably hope to ferret out the essential physics of the medium.

This exploratory survey will proceed under the assumption that the fundamental behavior of the corotating, 3-D solar wind may be ascertained from the analysis of a series of idealized models in which we manipulate

several influential factors about some prototype distribution of the free parameters on the source surface. Specification of the five dependent variables--u_r, u_θ, u_ϕ, ρ (or n), and P (or T)--on the source surface in a global format constitutes what we shall call the stream 'configuration'. In this paper we limit attention to input configurations of simple overall shape, describing smoothly varying high-speed streams that are surrounded by uniform slow flow. Given some prototype topology of the variations on the source surface, the nature of any configuration derived from the prototype may be characterized in terms of just five parameters:

1) The intrinsic correlations among the dependent variables (i.e., density-temperature-velocity correlations imposed at the source), as specified by the parameter, X, which is defined below.
2) The amplitude, A, defined in terms of the peak speed excursion about the slow flow state.
3) The longitudinal (azimuthal) scale of the configuration, Φ.
4) The latitudinal (meridional) scale of the configuration, Θ.
5) The central heliographic latitude of the configuration, λ_c.

This nomenclature is clarified in the discussion of the prototype stream, which follows immediately.

COMPUTATIONAL RESULTS

The Prototype Stream Configuration. In this subsection we define our prototype stream and describe the nature of its evolution to 1 AU. It will be thoroughly documented, for it has been accorded special significance as the standard reference example by which all the others shall be measured. It has been carefully selected on the basis that it exhibits a suitable cross-section of the effects we are interested in. Thus we may greatly simplify the later discussion by merely noting significant deviations from the norms established by the prototype.

The basic topology of our prototype stream at the source surface is closely patterned after (but is not exactly identical to) the example presented in Paper I. Figure 1 depicts contours of constant radial velocity projected onto the spherical source surface ($r_o = 35R_S$) with an incremental spacing of $\Delta = 30$ km/s. (North is at top, west is to the right,

so the structure is presented as one views the sun in the sky.) The radial velocity has a peak value of 580 km/s (marked by the H) and merges smoothly into the surrounding slow flow of 290 km/s. The full width of the variation across the center of the distribution, from slow flow to peak and back, corresponds to an arc of 60° on the source surface. The mathematical form of the variation is

$$u_r\,(r_o,\theta,\phi) = u_o(1 + Af) \tag{4}$$

where the amplitude, A, is defined as

$$A = \frac{(u_r)_{max} - u_o}{u_o} \tag{5}$$

and the angular distribution, f, is

$$f\,(r_o,\theta,\phi) = \left[\frac{\sin(\pi L)}{\pi L}\right]^2 \tag{6}$$

The quantity u_o refers to the slow-flow radial velocity. (For all the examples presented in this paper, the slow-flow conditions listed in Table 1 are used. The values at r_o were chosen to yield average conditions near 1 AU.) The quantity, L, is an arc along the source surface measured from the center of the distribution. Here the longitudinal and latitudinal scales are equal and the contours describe a circle centered at the equator; in general, though, L is a function of direction about the center of the distribution, and isocontours of f will describe an ellipse (e.g., see Figures 6 and 7). Thus, in terms of our nomenclature, the parameters for this stream read as follows:

$$A = 1.0,\ \Phi = \text{Ⓗ} = 60^{\circ},\ \lambda_c = 0^{\circ} \tag{7}$$

TABLE 1

PHYSICAL PARAMETERS FOR THE SLOW FLOW

	$r_o = 35R_S = 0.16$ AU	$r = 1.0$ AU
u_r(km/s)	290	401
u_θ(km/s)	0	0
$u\phi$(km/s)	0	0
$n(cm^{-3})$	370	7.1
$T(^oK)$	1.12×10^6	8.0×10^4
$P(dyne/cm^2)$	1.14×10^{-7}	1.59×10^{-10}

We have thus far expressed everything in terms of the radial velocity distribution at r_o. The nonradial velocity components u_θ and u_ϕ (defined in the inertial frame) are readily disposed of by noting that any nonradial flow imposed at r_o must decay as $1/r$, from conservation of momentum. Unless the nonradial motions imposed at r_o are unexpectedly large, they cannot compete with those which are driven by the stream interaction and grow rapidly with radius. Thus we set u_θ and u_ϕ equal to zero everywhere on r_o and concentrate only upon their evolution as it develops in the stream interaction. (In MHD models and for streams with radical geometries, more precise treatment of the input nonradial flows becomes mandatory and will be discussed in Paper III. For the broad HD structures presented here, the simplified approach above will suffice.)

Specification of the thermal state at r_o is not so straightforward, as we must proceed on the basis of inferences drawn from data collected well away from the sun. Long-term statistical evidence obtained by spacecraft near 1 AU appear to show an intrinsic positive correlation between temperature and velocity, while density and velocity are anti-correlated (Burlaga and Ogilvie, 1970, 1973; Barouch, 1977). However, these associations are somewhat compromised by the action of the very interplanetary processes we intend to study (Hundhausen, 1973a; Pizzo *et al.*, 1973). These effects can be minimized by considering only periods when the solar wind is approximately steady over a local expansion time from the sun to the point of observation. Studies of solar wind conducted in this manner (Feldman *et al.*, 1976; Neugebauer, 1976; and Bame *et al.*, 1977) lend credence to the view that high speed streams may be characterized as intrinsically hot, fast flow of low density, while the so-called "ambient" or "quiet" solar wind corresponds to intrinsically cold, slow flow of high density. This general picture of stream correlations has been confirmed by recent Helios observations as close as 0.3 AU. Indeed, these data suggest that the positive temperature-velocity and negative density-velocity correlations near the sun may be even more pronounced than heretofore supposed (Rosenbauer *et al.*, 1977).

Therefore, as a working hypothesis, we adopt the following relations at the source surface:

$$\rho(u_r)^X = \text{const} \tag{8a}$$

$$P = \text{const} \tag{8b}$$

where X is an adjustable parameter. [We emphasize that the constraints implied by (7)-(8) apply only on the surface r_o. The relations at larger radii are determined by the evolution of these conditions under the influence of interplanetary dynamics.] The case X = 0 corresponds to the example discussed in Paper I, i.e. a pure radial velocity variation with ρ, P, and T all held constant on r_o. For any X > 0, relation (8) guarantees that temperature and velocity will be intrinsically positively correlated, while density and velocity will be anticorrelated. Thus, the general shape of the ρ and T contours on a plot like Figure 1 are similar to those of u_r. The constancy of P as required by (8b) is an artificial constraint take for simplicity. Nevertheless, there is reason to expect that lateral pressure balance should pertain on a gross scale (see discussion of pressure-driven streams in section on correlations, below).

The case X = 1 implies a constant mass flux density across the stream at the source surface and is the value arbitrarily chosen for our prototype stream. This choice of X results in a relatively hot, tenuous, high-speed stream interacting with a surrounding cool, dense slow flow. Specifically, at the core of the stream, we have

$$\rho = \frac{\rho_o u_o}{(u_r)_{max}} = \frac{1}{2}\rho_o \tag{9a}$$

$$P = P_o \tag{9b}$$

$$T = \frac{\rho_o T_o}{\rho} = 2T_o \tag{9c}$$

Thus the prototype distribution at r_o is completely defined, and it remains only to propagate these initial conditions away from the sun by means of the numerical techniques outlined in Paper I.

The resulting prototype stream structure at 1.0 AU is presented in Figure 2(a-d), where we view the contours of constant radial velocity, number density, temperature, and pressure, respectively. Fast material at the core of the stream at r_o has overtaken the preceding slower material to

the west, steepening the radial velocity profile at its leading (right) edge (Figure 2a). The initially low densities in the stream core have been further depleted by the ensuing central rarefaction which arises as the fast material in the core outraces the slower material to the east (Figure 2b). Similarly, the temperature structure at 1.0 AU (Figure 2c) reflects its mixed history: the intrinsically hot gas at the stream core has been convected forward with the steepening, but the temperature is augmented at the leading edge due to compressional heating and is reduced in the trailing portions due to rarefactional cooling. Peak density and temperature are out of phase, with the former leading, while the gas pressure maximum lies between the two. This sequence is consistent with the observations (e.g., Burlaga et al., 1971; Siscoe, 1972; Gosling et al., 1972).

The pressure gradients built up in the stream interaction (Figure 2d) drive small nonradial flows. Since these flows arise entirely from the gas dynamics in this model, they attain their peak values in the regions of the steepest pressure gradients, which lie at the equator for the azimuthal component and at higher latitudes for the meridional component. Figure 3 shows the pattern of the nonradial flow at 1 AU superimposed on the pressure contours of Figure 2d. The small vectors are oriented in the direction of the tangential motions at 1.0 AU, with the length proportional to the magnitude. (Compare to the vector of 400 km/s, the minimum radial velocity, at bottom.) The vectors describe a general outflow directed away from the region of strong compression at the front of the stream and a general inflow directed towards the rarefaction. Because the motions are small, the actual displacement of fluid particles from radial propagation is negligible, amounting to just a few degrees to 1 AU. However, it was pointed out in Paper I that the nonradial flow is of major consequence to the competition between the kinematic and dynamic aspects of the evolution, despite the small overall amplitudes. This is because the flows always act to broaden the kinematically-induced pressure gradients and because they operate over a vast distance. Thus, while their local magnitudes may be small, their cumulative effects are large. A direct comparison of solutions (see Figure 11 of Paper I) demonstrated that neglect of the nonradial flow makes the 1-D model prone to serious error (at least inside 1 AU), while the 2-D model fares far better through inclusion of the east-west component.

An important objective of this paper is to consider in detail the nature of the purely meridional flow (3-D) effects in stream evolution. We begin by noting that, in assessing the influence of the north-south flow, it is insufficient to show only that the displacement of discrete fluid particles is negligible. The pattern of nonradial flow depicted in Figure 3 constitutes a vortex of global proportions, which results in the net latitudinal transport of energy and momentum, as well as mass. Furthermore, while mass may be transported at the flow speed (a phase-velocity phenomenon), information of the interaction at any given point propagates throughout the fluid at the local sound speed (a group velocity phenomenon). Thus the transport of energy and momentum may have more far-reaching effects.

There are basically two ways to evaluate the north-south transport: 1) on a local scale, by direct comparison of 2-D and 3-D solutions; and, 2) on a more extended scale, by actually computing the net latitudinal transport of conserved flux quantities.

We elect to consider the latter measure first. By casting equations (1-3) in flux conservation form and averaging over ϕ at fixed θ, we derive the flux-conservation relations

$$\vec{F}(r,\theta) + \vec{T}_{\theta}(\theta) + \vec{S}(\theta) = \vec{F}(r_o) = \text{const}, \tag{10}$$

where $\vec{F}$ is the conserved flux, $\vec{T}_{\theta}$ the integrated (between r_o and r) latitudinal flux transport, and $\vec{S}$ a source term. In the 3-D HD formulation, $\vec{F}$ is a five-vector whose components are

$$\vec{F} = \begin{bmatrix} \text{mass} \\ \text{radial mom.} \\ \text{meridional mom.} \\ \text{azimuthal mom.} \\ \text{total energy} \end{bmatrix} = \begin{Bmatrix} r^2 \rho u_r \\ r^2(\rho u_r^2 + P) \\ r^3(\rho u_r u_\theta) \\ r^3(\rho u_r u_\phi) \\ r^2\left[\frac{\rho}{2}(u_r^2 + u_\theta^2 + u_\phi^2) + \frac{\gamma}{\gamma-1} P\right] \end{Bmatrix} \tag{11}$$

We can evaluate the magnitude of the transport either by computing $\vec{T}_{\theta}$ directly or by comparing $\vec{F}$ at any (r,θ) with the equivalent 2-D solution for strip-wise identical source conditions. (This latter method eliminates

the minor confusion caused by the presence of the source term $\vec{S}$, which has only very small non-zero components in the radial-momentum and total energy equations.) For the mass, radial-momentum, and total energy flux-conservation quantities, we define the net percentage latitudinal flux transport as

$$\frac{\vec{F}(r,\theta) - \vec{F}(r_o,\theta)}{\vec{F}(r_o,\theta)} \times 100 \qquad (12)$$

The top panel of Figure 4 shows the percentage latitudinal flux transport of mass (M), radial momentum (D), and total energy (E) computed according to (12) as a function of colatitude, θ, across the prototype stream at 1 AU. (At bottom, there appears for reference a north-south slice along the central meridian of the input velocity structure.) First, we comment that the level of the transport amounts to only a few percent. This amplitude is of the same order as meridional transport effects predicted by axisymmetric theory (e.g., Nerney and Suess, 1975; Winge and Coleman, 1972) as arising from differential wrapping of the spiral magnetic field. Second, the two peaks in the distribution denote transport of flux from the equator toward higher latitudes. It is noteworthy that the greatest flux transport occurs at the equator, where the meridional velocity is zero, and at the poleward fringes of the structure, where the radial velocity amplitude is very low. Significantly, the null in the transport lies near $\theta = 75^{\circ}$, where the peak u_θ occurs. Thus the important factor here is the divergence of the flow, not the absolute value of the fluid velocity. The pattern of the transport is a strong function of source conditions, but the low level of the transport is expected to be a more general result. (The conserved fluxes M, D, and E are dominated by the radial kinetic terms; it is therefore difficult to see how they can be altered very much by the meridional flow.)

The azimuthal and meridional momentum transport is a more complicated issue. Because we start with no tangential momentum at r_o, we must adopt a modified criterion for judging the effects of the stream interaction on these two quantities. To facilitate the analysis, we cast the discussion in terms of the flux densities

$$L_{\theta,\phi} = r\rho u_r u_{\theta,\phi} \quad , \tag{13}$$

which can be directly related to observed momentum densities in the solar wind.

The longitudinally-averaged values of L_θ and L_ϕ are plotted as a function of θ at 1 AU in the center panel of Figure 4. Angular momentum has been transported polewards by the meridional motions induced in the stream interaction, with the result that the equatorial regions show a net anti-corotation, while the high-latitude fringes of the stream show positive corotation. The meridional flux density exceeds the azimuthal flux density because the imposed equatorial symmetry leads to predominantly polewards flow, while the east-west transport tends, on the average, to cancel out. Total angular momentum on a global scale still sums to zero (when we account for the small amount that has escaped polewards beyond the fringes of the computational mesh), but the vortex motion visible in Figure 3 has resulted in a redistribution of that momentum.

The absolute values of these flux densities are, however, quite small compared to typical (though still controversial) numbers quoted for the observed solar wind angular momentum, roughly 5×10^3 gm/s^2 at 1 AU (e.g., Lazarus and Goldstein, 1971). On face value, it is tempting to disregard the angular momentum transport due to streams as inconsequential. However, we must interject a note of extreme caution here, for the angular momentum flux densities (13) are directly proportional to the nonradial flow speeds and, unlike the M, D, and E fluxes, are not dominated by radial-kinetic contributions. In addition, our calculations include neither the magnetic field (which comprises roughly one-quarter of the total flux density at 1 AU) nor input angular momentum. This latter deficiency is especially worrisome, since most of the latitudinal transport occurs at the stream front, where any intrinsic correlations between stream structure and the angular momentum distribution may be strongly affected by the dynamics. Thus, at this juncture, we can only point out that an important effect may exist, and further quantitative estimates will have to await the MHD models of Paper III.

Finally, we return to the question posed above concerning the local effects of latitudinal transport upon stream evolution. Comparisons of 2-D and 3-D solutions reveal no useful, clearly identifiable differences

between the two formulations, except at the fringes of the stream where the amplitudes are uninterestingly low. Thus we have the important null result that the stream interaction proceeds very nearly as if confined to the east-west plane. However, this is not to say that the meridional flows are themselves unimportant. Indeed, as we have just seen, they may be of consequence for such subtle solar wind properties as angular momentum. Potentially more exciting are the prospects that we may learn to use measurements of u_θ obtained along the ecliptic to plumb the 3-D geometry of solar wind structure, since the pattern of these motions can be related to the large-scale flow topology. (We will return to this topic later.)

This concludes our discussion of the fundamental evolutionary properties of the prototype stream. In the following subsections, we systematically manipulate the input configuration about the standard reference prototype in an effort to isolate the effects of the five configuration parameters identified earlier. This set of model calculations covers the entire spectrum of stream types within the context of our parameter classification system.

The Stream Interaction as a Function of Density-Temperature-Velocity Correlations Imposed at the Source.

This subsection clarifies the role played by correlated thermodynamic variations imposed near r_o. To this end, we will consider the evolution of three model stream configurations in which we allow the correlation parameter, X, in (8a) to assume the values X = 0, 1, and 2, all other parameters being held constant. The case X = 0 corresponds to the velocity-driven stream of Paper I, X = 1 is the prototype configuration described above, and X = 2 examines the dynamics of a strongly correlated stream (e.g., at the center of the stream, $T = 4\ T_o$, $\rho = \rho_o/4$). [It is important to distinguish between the intrinsic correlations considered here and the induced correlations highlighted in Goldstein and Jokipii (1977). The latter arise out of the nonlinear nature of the stream-associated fluctuations. At any $r > r_o$, both intrinsic and induced correlations are present in the solution, though the former variety normally dominate.]

However, before we launch into the discussion of these results, we detour briefly for some important ancillary material. Specifically, it is instructive to learn what happens when temperature or density alone is varied at the source. Such input configurations imply unbalanced lateral

pressure gradients on the source surface, and we might expect the evolution of these structures to be of a different nature than that of the velocity-driven type. For brevity, we will simply quote some salient computational results for temperature and density-driven streams having all the same shape and scale configuration parameters as the prototype stream.

For the temperature-driven stream (of amplitude A = 1, here defined in terms of the peak excursion about the ambient temperature, T_o), we find that the input pressure enhancement quickly relaxes (spatially) toward overall pressure balance. The relaxation proceeds primarily in the radial direction because it is easier to drive material outwards into the tenuous reaches of space than laterally into adjoining regions which have densities comparable to that in the stream. The hottest material--that at the stream core--undergoes the greatest acceleration, leading to a marked depletion in the central density. Thus, within a very short distance of the source surface, the initial pure-temperature variation is transformed into a stream of modest velocity amplitude which is characterized by fast moving material that is hot and rarified relative to the cool, dense, slow-moving medium that surrounds it. The nonradial flow induced in the initial relaxation subsequently decays due to geometric effects and beyond several tenths of an AU from the inner boundary becomes negligible compared to the large deflections built up in the ensuing stream evolution. Beyond this point, the familiar rotational interaction mechanism governs the evolution and the structure propagates to 1 AU as a low-amplitude version of the prototype stream.

A steady density enhancement at the inner boundary also represents a pressure perturbation, but with one very significant difference from the temperature-driven case. Namely, the importance of the pressure forces is substantially diminished by the increased mass in the flow. Hence motions generated by this configuration are tiny indeed, with perturbations in all three velocity components on the order of a few km/s. Because the induced flows are small, the rotational interaction is negligible and the resultant structure at 1 AU is manifest as a broad, cool, low-amplitude density enhancement attended by only minor, inconspicuous velocity fluctuations.

Therefore we have not necessarily forfeited much generality in adopting the correlations (8). Density-driven streams, in themselves, are not of much dynamical interest, while temperature-driven streams quickly

relax into a configuration remarkably similar to our prototype model. Naturally, when we combine these variations in one configuration, the inherent nonlinearities prevent simple addition of effects. It is just this coordinated behavior we now investigate as we return to the main line of our exposition.

To reiterate, in the remainder of this subsection we will compare solutions at 1 AU for model streams with the parameter X equal to 0, 1, and 2. It will not be necessary to present global displays for each stream, as the general patterns of the solutions are similar to those in Figure 2. Rather, we focus attention upon the evolution in the vicinity of the equatorial plane, where the meridional divergences are largest. Figure 5 contains plots of the important plasma parameters along the equator in time-sequence form, simulating the data format of a spacecraft in earth orbit. (Note that this spacecraft convention corresponds to scanning the contour plots, as in Figure 2, from right to left. Conversion from the angular units of the display to temporal units may be effected by using the synodic solar rotation rate of 13.3^{o}/day.) In each panel, the solid line refers to the prototype X = 1 solution, the dashed line to X = 2, and the dotted line to X = 0.

The first feature of Figure 5 to be pointed out is how the relative amplitude (in terms of the radial velocity, top panel) increases with X. This is a consequence of imposing the correlations (8) at r_o. The larger central temperatures associated with increasing X imply more thermal energy content per particle and lower effective mach number at the source. Hence, the material at the stream core experiences significant radial acceleration, even though the pressure is held constant on r_o. The higher velocities dictate a more rapid evolution, but the augmented kinematic steepening is in turn vitiated by the nature of the momentum distribution across the stream. That is, as X increases, the intrinsic central density declines and the compressed gas at the leading edge is able to more effectively react back on the high-speed portions of the stream. This process is further amplified by the elevated temperatures in the stream core, which imply larger sound speeds and result in dispersal of the compressive stresses over a greater volume. Therefore, despite the fact that the X = 2 trough-to-peak velocity amplitude is nearly 400 km/s over a short span of longitude, the stream has not shocked inside 1 AU.

This whole process merits closer attention. The discussion is most conveniently conducted in terms of the radial momentum flux density

$$\mathfrak{F} = \rho u_r^2 + P, \tag{14}$$

which has both kinetic and thermal components (and magnetic components in the full MHD formulation). This quantity is of paramount importance to stream dynamics, for variations in the momentum density couple with rotation to define the character of the interaction. For X = 0, the correlations (8) imply constancy of ρ and P all the way across the stream at r_o. Hence, by virtue of the high radial velocity in the stream core, the momentum flux density in the stream far exceeds that in the slow flow and the interaction is dominated by kinematic effects. The high-speed material overwhelms the slow gas caught in the squeeze, in the classic "snowplow" picture of stream steepening. However, as X increases, the ratio of $\mathfrak{F}$ in the stream to $\mathfrak{F}$ in the slow flow declines, and the dynamic aspects of the interaction are enhanced. At X = 2, a natural break in behavior is realized, since the radial momentum flux density at the source surface is the same both within and without the stream. At this point, the slow flow material begins to exert commanding influence on the course of the evolution. Indeed for X > 2, the interaction approaches the logical antithesis of the snowplow model, namely, that of an exceedingly hot and tenuous gas colliding with a cold, massive, unyielding ambient, in what may be alluded to as the "brick wall" limit. One can speculate that were this scenario the more physically applicable one, then it would be the properties of the imperturbable low-velocity structure that would excite our interest, rather than the wispy high-speed portions of the flow. However, our prototype stream (and, apparently, the real solar wind) occupies a niche somewhere between these two very different extremes.

The relative phase and amplitudes of the thermodynamic variables (next three panels of Figure 5) correspond in no simple way with the radial velocity amplitudes, for they are the complex product of intrinsic variations modified by interplanetary processes. For the X = 0 case, density and temperature are exactly in phase and deviations from the slow-flow values are entirely due to the compressive effects of the stream interaction. As X increases, however, the intrinsic component of the

thermodynamic variations becomes visible: the density peak shifts forward relative to the temperature peak, with the pressure maximum lying between. The amplitude of the density and pressure change little despite the large range of radial speeds in the three examples, though there is a tendency for the density peak in the highly dynamic X = 2 case to be somewhat sharper than in the more kinematic X = 0 case. The temperature alone shows a clear progression from X = 0 to X = 2.

The fifth panel of Figure 5 displays the azimuthal velocity curves for the three examples. These variations describe a strong east-west shear aligned along the stream front and centered upon the pressure ridge. (Away from the equator there is also a north-south component to the shear.) The positive (westward) deflection changes only modestly in response to the different values of X, while the negative deflection increases dramatically at large X. The reason is that conditions in the slow flow just ahead of the stream are similar in each case, while those well back in the compression region are strongly influenced by the intrinsic thermodynamic properties. For large X, the low densities in the stream core mean that the pressure forces there operate on material with reduced inertia, and therefore produce larger deflections. The last panel in Figure 5 simply records these deflections in terms of flow angle in the inertial frame:

$$\psi = \arctan\left(\frac{u_\phi}{u_r}\right).$$

Since u_r is inherently larger in the region of negative u_ϕ, the solutions for increasing X yield a more symmetric variation of flow angle about the stream front, which corresponds more closely to the observations.

The relation of intrinsic parameter correlations existing near the sun to the structure of stream interfaces observed near 1 AU has been the subject of 1-D calculations (Hundhausen and Burlaga, 1975). These features occur often near stream fronts and may be characterized as a rapid transition from slow, cold, dense flow to hot, fast, tenuous flow across a narrow shear layer. The interfaces pictured in Figure 5 are more closely akin to the broad structures discussed by Burlaga (1974) than to the near-discontinuities reported by Gosling et al., (1978). Our calculations illustrate how the interface becomes more pronounced as the input

correlations become more extreme. This enhancement comes about partly through simple mapping of source conditions and partly through more vigorous heating of the tenuous gas in the stream relative to that of the dense gas comprising the slow flow (Gosling et al., 1978). The shear flow arises from the stream-induced pressure gradients and develops whether or not a true interface is present (i.e., shear accompanied by sharp density and temperature transitions). However, the shear is considerably intensified at large X, owing to the enhanced dynamic reaction of the low-density, high-speed material.

The meridional transport properties of the stream interaction are influenced by the input parameter correlations, but the overall effects remain small. Table 2 records the extreme values of the nonradial velocities and latitudinal transport of the conserved fluxes and flux-densities at 1 AU for the three values of X. (In Tables 2-6, the values for each parameter do not necessarily pertain to the equator, but represent the extreme occurring anywhere within the stream. Owing to the symmetry of the examples, the general patterns of the parameter variations follows those of the prototype stream: u_ϕ has both extrema at the equator; M, D, E and L_ϕ have minima at the equator, maxima at higher latitudes; and L_θ has a single extrema at mid latitudes. The u_θ parameter is treated as a special case, with both tabulated extrema lying in the northern hemisphere only, one referring to the deflection at the stream front, the other to that in the rarefaction.) The disparity between the behavior of the peak azimuthal and meridional deflections (u_θ is much less sensitive than u_ϕ to changes in X) further evidences the loose coupling of the meridional motions to the stream interaction. The flux transport statistics are surprising in that the net latitudinal transport depends inversely upon X, whereas most of the parameter amplitudes are oppositely related. Two factors contribute to this result: 1) owing to the greater intrinsic density of the high-speed material at low X, there is simply more flux in the stream to participate in the transport; and, 2) due to the lower intrinsic density of the high-speed material at large X, an increasing fraction of the momentum exchange in the interaction region is channeled into local heating of the flow rather than into deflection (though the deflection is also enhanced).

For brevity, we will assert without graphical display that 2-D solutions executed for the source conditions obtaining along the equator produce minimal deviation from the 3-D predictions at 1.0 AU. In light of the above discussion, we therefore conclude that the input parameter correlations exert far more influence on the appearance of a stream at 1.0 AU than do the geometric factors attributable to 3-D as opposed to 2-D flows.

TABLE 2

STREAM PARAMETERS AT 1.0 AU AS A FUNCTION OF X

	X = 0	X = 1	X = 2
Peak Values Anywhere within Stream (max/min)			
u_θ (km/s)	5.6/-14.2	7.2/-16.0	9.6/-18.4
u_ϕ (km/s)	28.4/-17.9	27.4/-36.1	34.6/-69.0
M (%)	2.23/-3.64	1.38/-2.26	0.12/-0.22
D (%)	2.67/-4.21	1.54/-2.67	0.13/-0.17
E (%)	2.71/-4.18	1.56/-2.73	0.47/-0.35
L_θ (x $10^3 gm/s^2$)	$\pm$ 1.01	$\pm$ 0.61	$\pm$ 0.23
L_ϕ (x $10^3 gm/s^2$)	0.06/-0.13	0.06/-0.12	0.08/-0.16

The Stream Interaction as a Function of Input Amplitude.

The input amplitude, A, affects the evolution of a stream in two ways. First, higher amplitudes imply sharper longitudinal gradients at the source, which lead to more rapid steepening through the usual rotational interaction. Second, higher amplitudes normally mean that the material in the stream carries higher momentum flux density than that outside and thus the stream packs more inertia with which to maintain that steepening. Hence the evolution of high amplitude streams is expected to proceed more swiftly and with increased likelihood of shock formation.

To quantitatively assess these amplitude effects, we have executed a series of examples in which A assumes the values 0.5, 1.0 (the standard prototype), and 2.0, all the other stream parameters being held constant. It is especially important to bear in mind that the correlation parameter here has the value X = 1, and therefore while the initial pressure across the stream is held constant, the initial temperature and density vary according to relations (8). The consequences of this property will become apparent shortly.

The contour patterns at 1 AU for all three streams in the amplitude series are quite similar to those of the prototype in Figure 2, and all the essential features of our intercomparison are summarized in Table 3. Here we present the extreme values of the plasma parameters and the latitudinal flux transport occurring anywhere within the stream. It can be seen that the amplitudes of the various parameters at 1.0 AU increase with A, but not so sharply as might be expected on the basis of simpler kinematic and 1-D models. The nonlinearities in the evolution have been partially masked by the mapping of the boundary conditions, and the increased kinematic steepening at large A has been partially countered by the enhanced dynamical broadening properties associated with the hot, tenuous conditions within the stream.

The same momentum arguments outlined in the discussion attending equation (14) also apply here. Higher speed amplitude always implies that the rate at which material is brought into the interaction region is increased. On the other hand, the radial momentum flux density balance depends on the density-temperature-velocity correlations. Fox X < 2, higher amplitude means enhanced radial momentum flux density, $\mathcal{F}$, in the stream. (Again, we are speaking strictly of the input correlations at the

source surface.) However, for X > 2, high amplitude actually implies lower $\mathcal{F}$ in the stream, and the interaction is ever more dominated by dynamic, as opposed to kinematic, processes. The very rapid radial expansion associated with such a stream near the sun would be substantially degraded through momentum transfer with the slow flow within a short radial span, and an observer near the earth would likely see only a very eroded, feeble remnant. Regardless of whether the actual correlations in the upper corona are so simple or consistent as our hypothetical relations (8), the essential point to be drawn is that amplitude-dependence of stream evolutionary behavior is a much more complicated proposition than simple kinematic considerations might lead one to believe. Large velocity amplitudes do not necessarily imply large density and temperature perturbations at 1 AU, nor do they necessarily imply a greater tendency toward shock formation, for the intrinsic density-temperature-velocity correlations affect the dynamic balance in the compression region to a significant degree.

Finally, Table 3 shows that the meridional flow effects are surprisingly insensitive to changes in amplitude. The response of both u_θ and the latitudinal transport parameters are nearly linear with A, and remain small in each case. Hence, even for large-amplitude streams, the 2-D flow approximation retains considerable validity.

TABLE 3

STREAM PARAMETERS AT 1.0 AU AS A FUNCTION OF A

	A = 0.5	A = 1.0	A = 2.0
Extrema Anywhere within Stream (max/min)			
u_r (km/s)	543	689	983
u_θ (km/s)	4.8/-8.2	7.2/-16.0	13.3/-31.0
u_ϕ (km/s)	12.5/-16.7	27.4/-36.1	69.5/-90.2
n (cm^{-3})	10.5/3.9	15.2/2.7	29.6/1.7
T ($\times 10^3 {}^oK$)	151/70	255/64	576/60
P ($\times 10^{-10}$ dyne/cm^2)	3.9/0.85	8.2/0.59	24.7/0.44
M (%)	0.78/-1.32	1.38/-2.26	2.29/-3.50
D (%)	0.85/-1.54	1.54/-267	2.56/-3.88
E (%)	0.831/-1.57	1.56/-2.73	2.75/-3.62
L_θ ($\times 10^3$ gm/s^2)	$\pm$ 0.29	$\pm$ 0.61	$\pm$ 1.27
L_ϕ ($\times 10^3$ gm/s^2)	0.01/-0.02	0.06/-0.12	0.24/-0.52

The Stream Interaction as a Function of the Longitudinal Scale.

Under our nomenclature, the longitudinal scale of a stream, Φ, is defined as the total breadth of the structure in the azimuthal direction from where it first departs from slow conditions to where it returns to them. In assessing how the input breadth regulates the evolution, we must take into account three separate factors. First, the azimuthal gradients dictate the rate at which the interaction proceeds. All other factors being held constant, these gradients are inversely proportional to the longitudinal scale. Second, the total amount of stream material (or, momentum) available to participate in the interaction is directly proportional to the longitudinal scale. And third, because the interaction takes place in a supersonic medium, finite propagation effects must be considered. That is, only the leading edge of a stream is directly involved in the exchange of momentum between fast and slow flows, and it takes time for news of the interaction to propagate back into the main body of the stream. Taken together, these three factors assure that a longitudinally-narrow (small Φ) stream not only evolves more rapidly, but also the entire structure is quickly consumed in the interaction. Conversely, a longitudinally-wide (large Φ) stream evolves more slowly and carries more momentum with which to maintain that evolution over large radial distances.

In Table 4, we compare parameter variations at 1 AU for streams having a range of input longitudinal scales, Φ, equal to 30°, 60°, and 90°. The radial velocity structure at $r_o = 35R_S$ for the three examples of Table 4 is schematically indicated in Figure 6, which shows the rather discordant geometries involved: the $\Phi = 120^{\circ}$ case represents an oblate distribution, while the $\Phi = 30^{\circ}$ case possesses a prolate symmetry.

TABLE 4

STREAM PARAMETERS AT 1 AU AS A FUNCTION OF INPUT LONGITUDINAL SCALE, Φ

	$\Phi = 30^{\circ}$	$\Phi = 60^{\circ}$	$\Phi = 120^{\circ}$
	Extrema Anywhere Within Stream (max/min)		
u_r (km/s)	657	689	701
u_θ (km/s)	10.4/-18.4	7.2/-16.0	4.7/-10.3
$u\phi$ (km/s)	41.0/-73.0	27.4/-36.1	11.2/-8.8
n (cm^{-3})	16.9/2.4	15.2/2.7	10.7/3.1
T ($\times 10^{3}{}^{o}K$)	271/59	255/64	198/72
P ($\times 10^{-10}$ dyne/cm^2)	8.4/0.46	8.2/0.59	4.8/0.81
M (%)	1.57/-2.26	1.38/-2.26	1.21/-2.07
D (%)	1.71/-2.30	1.54/-2.67	1.37/-2.68
E (%)	1.63/-2.13	1.56/-2.73	1.48/-2.90
L_θ ($\times 10^{3}$ gm/s^2)	$\pm$ 0.71	$\pm$ 0.61	$\pm$ 0.47
L_ϕ ($\times 10^{3}$ gm/s^2)	0.20/-0.39	0.06/-0.12	0.01/-0.02

Table 4 supports the introductory statements made above. The $\Phi = 30^{\circ}$ stream is highly evolved at 1 AU with much of the radial kinetic momentum having been dissipated in a large compression (peak u_r down to 657 km/s) and strong azimuthal shear flow at the leading edge. At 1 AU, the $\Phi = 60^{\circ}$ prototype stream is also driving a vigorous compression, but because the steepening is occurring farther from the sun the lower sound speed and more nearly radial orientation of the stream front gradients are inhibiting the build-up of the azimuthal flows. The evolution of the $\Phi = 120^{\circ}$ stream has barely commenced at 1 AU, where kinematic effects are still dominant.

Table 4 also confirms the findings of linear theory (Siscoe and Finley, 1972) that the meridional effects are not particularly sensitive to the azimuthal scale. The meridional velocity is small in all three cases due to the interplay of the geometry with the dynamics: while the $\Phi = 30^{\circ}$ stream evolves rapidly near the sun where nonradial flows are most efficiently driven, the input latitudinal gradients are, by construction, relatively small (i.e., the contours are predominantly north-south); on the other hand, the $\Phi = 120^{\circ}$ stream evolves so slowly that the higher input latitudinal gradients have little effect inside 1 AU. As a result, the latitudinal transport parameters remain insignificant in all these cases.

The Stream Interaction as a Function of the Latitudinal Scale.

From the standpoint of 3-D effects, a far more interesting situation arises when we directly manipulate the latitudinal gradients. In Figure 7, we schematically illustrate a sequence of three input stream geometries characterized by variations in the latitudinal scale, Θ. ($\Phi = 60^{\circ}$, as usual.) For the $\Theta = 120^{\circ}$ case, the stream front runs nearly north-south and we expect minimal meridional flow effects; this stream closely approximates the idealization implicit in 2-D models. The $\Theta = 30^{\circ}$ stream embodies the topological opposite: an elongated east-west ellipse, with very substantial gradients (up to 30 km/s/deg) in the north-south direction. This stream provides us with an excellent test for meridional flow effects: not only does the structure have steep north-south gradients over most of its longitudinal width, but the full latitudinal span is comparatively modest. The boundary conditions at the equator are identical in all three cases. Hence this triad of examples allows us to view unambiguously the influence of meridional gradients.

The usual stream parameters at 1 AU are summarized in Table 5. We find that the peak u_θ is only mildy sensitive to the latitudinal scale and that the effects of the meridional flow are confined to minor systematic adjustments in the various parameters. That is, as θ_0 decreases, the north-south flows resulting from the stream interaction become slightly more efficient in moving material away from the region of the most intense compression and therefore the peak density at the equator is reduced while the peak radial velocity is increased. We furthermore declare that the stream profiles at the equator do not otherwise differ appreciably among the three cases. Thus these examples explicitly document the claim that meridional flow effects in the interplanetary solar wind are apt to be quite small, even in the limit of fairly extreme latitudinal gradients.

TABLE 5

STREAM PARAMETERS AT 1 AU AS A FUNCTION OF INPUT LATITUDINAL SCALE,

	$\Theta = 30^{\circ}$	$\Theta = 60^{\circ}$	$\Theta = 120^{\circ}$
	Extrema Anywhere within Stream (max/min)		
u_r (km/s)	692	689	686
u_θ (km/s)	9.2/-20.2	7.2/-16.0	4.6/-10.4
u_ϕ (km/s)	28.0/-33.6	27.4/-36.1	30.3/-38.5
n (cm^{-2})	14.4./2.9	15.2/2.7	15.9/2.6
T (x 10^{3}°K)	252/70	255/64	263/61
P (x 10^{-10} dyne/cm^2)	7.6/0.75	8.2/0.59	8.9/0.53
M (%)	1.26/-2.83	1.38/-2.26	0.80/-0.79
D (%)	1.32/-3.41	1.54/-2.67	0.91/-0.92
E (%)	1.24/-3.83	1.56/-2.73	0.91/-0.89
L_θ (x 10^3 gm/s^2)	± 0.43	± 0.61	± 0.53
L_ϕ (x 10^3 gm/s^2)	0.09/-0.18	0.06/-0.12	0.03/-0.05

The Stream Interaction as a Function of the Source Latitude.

The final parameter affecting stream evolution is the heliographic latitude of the source center, λ_c. Because the component of solar rotation acting on a fluid element situated at some latitude λ decreases as λ approaches $\pm 90^o$, the stream interaction is said to weaken with heliographic latitude. The rotational dependences goes as cos λ (or, sinθ), and, hence the differential north-south evolution across most streams due to the geometric effect will be small, particularly in the vicinity of the equator.

It is possible to discuss this effect in a way more closely related to the previous exposition and, at the same time, to clear up a potential point of confusion. The sharp-eyed reader will have noticed that the rotation term, $-\Omega\ \partial/\partial\phi$, in the governing equations (1-3) contains no explicit reference to θ. These equations have been specialized to the inertial frame and the true θ-dependence is masked in this form. For this reason, it is advantageous to discuss the latitudinal effect from the standpoint of spatial and angular scales. If we were to move our prototype distribution polewards while keeping all spatial scales constant, then the angular scale across any azimuthal (longitudinal) cut through the distribution must increase. On the other hand, were the angular scale held constant as the distribution is moved polewards, then the spatial scale in the longitudinal direction must decrease. Applying the experience of the subsection on longitudinal scale, we anticipate that the evolution of a high-latitude stream in the former case (fixed spatial scale) would tend toward that of a long-period (large Φ) stream, while the evolution in the latter case (fixed angular scale) would approach that of a short-period (small Φ) stream. (In neither instance will the analogy be exact, however, for the convergence of the geometry near the poles affects not only the rotation term in the equations, but also the divergence terms. Indeed, these secondary geometric considerations give rise to a fundamental property of flow about a sphere, namely, that the presence of any east-west structure must inevitably lead to north-south flows. However, it is not true that north-south structure must lead to east-west flows, a fact exploited in axisymmetric models.)

The best way to quantify these arguments is by means of a series of model streams at various latitudes, as illustrated in Figure 8. Here we

view the radial velocity contours at r_o = 0.16 AU for otherwise identical streams centered at $\lambda_c = 0^o$, $+45^o$, and $+90^o$, respectively (Figure 8 top). (The left-most example is the familiar prototype stream of Figures 1 and 2.) Figure 8 (middle) shows the radial velocity contours at 1.0 AU, while Figure 8 (bottom) highlights the pressure contours at 1.0 AU. A scan of these plots quickly reveals the dominant role of rotation in the stream interaction. The polar stream, for which Ω is effectively zero, displays none of the evolutionary artifacts usually associated with stream dynamics. The parameter variations have been essentially mapped to 1.0 AU, with only minor changes attributable to residual entropy differences within the stream. (Note the change of scale, Δ, for the pressure plot of the polar stream.) The equatorial stream, on the other hand, has been strongly affected by the dynamics and the characteristic compression-rarefaction pattern is evident. The stream at intermediate latitude ($\lambda_c = 45^o$) is still primarily rotation-dominated ($\cos \lambda_c = 0.707$). Though it is not very noticeable in the Figure, there is some differential evolution between polewards and equatorwards portions of this stream. That is, the northerly portions suffer less stream interaction than the southerly portions by virtue of the sizeable differences in λ, and hence the north-south symmetry is partially destroyed.

TABLE 6

STREAM PARAMETERS AT 1 AU AS A FUNCTION OF SOURCE CENTRAL LATITUDE, λ_c

	$\lambda_c = 0^\circ$	$\lambda_c = +45^\circ$	$\lambda_c = +90^\circ$
	Extrema Anywhere within Stream (max/min)		
u_r (km/s)	689.	699	707
u_θ (km/s)	7.2/-16.0	5.6/-11.8	$\pm$ 1.66
u_ϕ (km/s)	27.4/-36.1	17.2/-20.1	0.0
n (cm^{-3})	15.2/2.7	11.6/3.0	7.1/3.5
T (x $10^3{}^\circ K$)	255/64	208/69	160/80
P (x 10^{-10} dyne/cm^2)	8.2/0.59	5.2/0.74	1.64/1.57
M (%)	1.38/-2.26	1.39/-1.48	-11.9*
D (%)	1.54/-2.67	1.51/-1.93	-12.9*
E (%)	1.56/-2.73	1.40/-2.13	-17.9*
L_θ (x $10^3 gm/s^2$)	$\pm$ 0.61	0.36/-0.31	0.0*
L_ϕ (x $10^3 gm/s^2$)	0.06/-0.12	0.02/-0.03	0.0*

*measured at pole only

Table 6 presents the parameter variations at 1.0 AU for the three streams of Figure 8. Here the transport parameters for the polar stream have been measured exactly at the pole. In contrast to the latitudinally-averaged figures quoted for the equatorial and mid-latitude streams, the flux loss recorded for the polar stream is much greater because it refers to the local depletion occasioned by the perfectly symmetric divergence of material about the stream core. Similar transport of flux occurs locally within equatorial stream fronts (indeed, local azimuthal transport is the prime broadening agent in streams), but losses and gains tend to balance out across the structure, making for a small net value.

While the evolutionary behavior of streams changes dramatically between pole and equator, the transition between the two regions is smooth and the physics of the mechanism relatively straightforward. The latitudinal dependence of stream evolution is rather weak, especially in the vicinity of the equator, and hence calculations executed for a stream situated at the equator (the preferred location, for numerical purposes) are really applicable over a broad band of latitudes.

A PRACTICAL EXAMPLE: The Trans-Equatorial Extension of a Polar Hole.

In the previous sections, we have reviewed the action of the five basic factors in stream dynamics on an individual basis within the context of a particularly simple, symmetric geometry. Unfortunately, the corona is seldom so aesthetically ordered. Therefore, we present one example that combines all these features in an asymmetric configuration of practical interest. It is intended to be suggestive of one of the more common coronal topologies witnessed during the Skylab period, namely, a polar hole with an extension jutting down across the equator (e.g., Bohlin and Rubenstein, 1975). We shall use this example to demonstrate the generality of our previous results and to dispel any lingering doubts that might have emerged over our past reliance upon perfectly symmetric configurations. Also, it will be of assistance in illustrating some additional 3-D concepts we wish to introduce.

Figure 9 displays the radial velocity contours for the asymmetric stream on the source surface $r_o = 0.16$ AU. The correlations (8) are again imposed (with $X = 1$), so the contours of density and temperature have a

geometry similar to Figure 9. The nonradial velocity components at r_o are set to zero, and the pressure is constant. The distribution depicted represents a uniform, hot, tenuous high-speed flow about the north pole, having a lobe-like trans-equatorial extension. Everywhere southward of the u_r = 300 km/sec contour, the flow is that of the standard conditions of Table 1. (The entire structure repeats every 120° in longitude for numerical purposes; however, the periodic interaction is negligible at1 AU, except at high latitudes, where the stream is already broad and of low relative amplitude.) Both the amplitude and azimuthal span of the stream increase rapidly with latitude (moving north), and the variations at the equator are identical with those of the standard prototype stream. However, we have now sandwiched those equatorial boundary conditions in the midst of a highly nonuniform geometry.

The contours of constant radial velocity, density, temperature, and pressure at 1.0 AU are presented in Figure 10(a-d). The overall shape of the structure has not changed appreciably, but the stream-front steepening is evidenced by the close spacing of velocity contours at the western (right) edge. A strong compression has formed diagonally across the equator and is centered somewhat to the north because of the higher input amplitude of the stream at those latitudes. The variations in the thermodynamic parameters n, T, and P reflect the influence of the interplanetary dynamical processes upon their initial, large-amplitude, global distribution. Thus n, T, and P are all out of phase and peak at slightly different locations.

The pattern and magnitude of the nonradial flow at 1.0 AU are defined in the velocity vector diagram (Figure 11). The vectors are projected against the pressure contours of Figure 9d, their length being proportional to their magnitude. Again we witness a general tangential divergence of material away from the compression and into the ensuing rarefaction.

Despite all the asymmetry and the strong latitudinal gradients characterizing this stream, the 3-D effects remain small, as in our previous examples. This claim is substantiated in three ways. First, it is evident from Figure 11 that the nonradial velocity is quite low relative to the radial expansion speed. By tracing the motion of selected marker particles imbedded in the flow, it can be established that these nonradial flows lead to little north-south displacement of fluid elements. Figure 12

shows a grid of such marker particles at 1 AU, as distorted by the rotational interaction and the resultant nonradial flows. (At r_o, the particles were arrayed in a uniform 5^o x 5^o grid. The dotted lines link the points in their original sequence.) Compressions and rarefactions are clearly reflected in the relative marker particle densities. The density contours of Figure 10b are provided for reference, but note that the contours represent the combined effects of intrinsic variations and interplanetary re-arrangement of material. It is apparent that the meridional displacements are restricted to a few degrees, even in the region of the stream front. Second, the longitudinally-averaged latitudinal flux transport is negligible, as documented in Figure 13. There has been a general divergence of mass, energy, and momentum towards the equator, but this transport is of limited proportions and therefore of minimal global significance. And third, it can readily be shown that the latitudinal transport is of no local importance, either. Figure 14 compares 2-D and 3-D solutions in the equatorial plane at 1 AU. From the top, the panels display simulated spacecraft sequences of the radial velocity, density, temperature, pressure, and nonradial velocity variations, respectively. No significant deviations between 2-D and 3-D solutions occur, even though the equatorial region lies astride the steepest latitudinal gradients. Thus it seems safe to conclude as a general rule that the amount of stream spreading in interplanetary space is insignificant and that any large-scale latitudinal gradients impressed upon the flow near the sun are likely to survive well out into the solar system.

Meridional Flow Variations as a Diagnostic Tool.

The only identifiable signature of the 3-D flow topology that can be observed by spacecraft operating in a narrow latitudinal band resides in the pattern of the meridional flows at the leading edge of a stream. Our presentation of the asymmetric stream has been motivated, in part, by our intention to demonstrate how 3-D modeling techniques may be applied to the analysis of solar wind data collected near the ecliptic plane. We shall eschew quantitative arguments in favor of a qualitative outline of the essential aspects of the proposed method. (This topic will be treated more fully in Paper III.)

Within the context of the purely pressure-driven tangential motions described in this paper, there exist just two basic classes of stream-associated meridional flows: edge flows and direct-driven flows. These are most easily defined in terms of diagrams. The top panel of Figure 15 depicts schematic representations of ideal edge flow (a) and ideal direct-driven flow (b). Contours of constant pressure at 1 AU are drawn for two hypothetical stream fronts, and the short, open arrows in each case mark the local direction of the induced nonradial flows. The heavy dashed arrow sweeping horizontally across the contours from right to left (west to east) indicates the temporal sequence of variations that would be observed by a spacecraft at that latitude as the pattern corotates past it.

The recorded variations in the azimuthal and meridional velocities are sketched in the bottom panel of Figure 15. The simulated data describe two distinct patterns of meridional flow. In the case of the perfect, idealized edge flow (a), the meridional motions are of an entirely secondary nature, deriving only from latitudinal variations in the intensity of the east-west stream interaction, i.e., from gradients along the stream front. This kind of flow exhibits a characteristic phase shift between the meridional and azimuthal variations, as shown in Figure 15a (bottom). The meridional velocity peaks as the azimuthal velocity swings rapidly from east to west across the pressure ridge. In the idealized direct-driven flow (b), the meridional motions are tightly coupled to the stream interaction and owe their existence to the inclination of the front from the meridional plane. Therefore, the direct-driven flow has both meridional and azimuthal velocity variations in phase, as illustrated in Figure 15b (bottom). In general, of course, the phase shift may fall anywhere between these two extremes, depending upon the topology of the stream. For example, the meridional flow arising from the prototype stream (Figure 3) is predominantly of the edge-flow variety, while the asymmetric stream (Figure 11) induces predominantly direct-drawn flows (c.f. bottom panel of Figure 14). Thus we have at our disposal a potentially useful diagnostic tool that follows as a natural consequence of the large scale pressure distribution that dynamically evolves in the stream interaction.

The word 'potentially' qualifies our statement, however, for obstacles remain. Observations of the flow velocities alone lead to ambiguous

perception of the topology of the stream structure. For example, throughout most of the latitudinal span of the asymmetric stream, the stream front is preceded by north-to-south flow, indicative of a structure that lies generally north of the observer (see Figure 11). On the other hand, above + 25°N latitude, the preceding north-south flow is so slight as to be lost in the statistical noise, and an observer, cognizant only of the more appreciable south-north flow coming off the back of the interaction ridge, might wrongly deduce that the stream lay generally to the south. (One can easily imagine more complicated stream configurations to aggravate the problem.) The root of the confusion is that the nonradial flow responds to stream gradients and not to stream magnitude, per se. Attempts to bring quantitative aspects of the problem into play are similarly fraught with uncertainty. If meridional flows were purely of the direct-driven type, the tilt of the front with respect to the local meridian could be inferred from the ratio of the amplitudes of the meridional and azimuthal components (e.g., Siscoe and Sullivan, unpublished manuscript). However, the contributions of edge flows could be sizeable, especially if the north-south boundaries of streams are relatively sharp. At present, it is not clear how to separate the two components.

Hopefully, knowledge of both the amplitude and phase of the nonradial velocity variations, used in conjunction with the information contained in the magnetic field variations, may alleviate these difficulties. MHD models will provide a more reliable estimate of flow velocities and permit investigation of possible tell-tale plasma-field correlations. Observations of the field polarity could help resolve the directional ambiguities mentioned above by establishing the likely hemispheric origin of the plasma. Clearly, this is a complex topic and should be a prime objective of future 3-D MHD studies.

SUMMARY AND DISCUSSION

We have examined in some detail the 3-D hydrodynamic interaction of corotating solar wind streams. To reduce the inherent complexities of such a system to a tolerable level, we have sought to resolve the most important features of the process down to a few readily tractable elements. Specifically, we have emphasized the simplication and coherence of discussion that

results when one views any given stream configuration as a stationary corotating wave whose primary properties are the longitudinal radial velocity gradients (which govern the rapidity of the evolution) and the distribution and partitioning of momentum (which together regulate the course and extent of the evolution). We have seen that by suitably manipulating these properties near the sun in a variety of ways, we can profoundly affect the balance between the kinematic tendency of high-speed streams to steepen and the dynamic reaction of the medium to resist further compression.

The plasma variations seen in the solar wind partly reflect intrinsic coronal conditions convectively mapped into space and partly reflect interplanetary modifications acquired in the stream interaction. In the classical snowplow concept of stream dynamics, the kinematic steepening process dominates the evolution and the intrinsic thermodynamic and magnetic components assume a passive role. The high densities seen along stream fronts are then attributed almost entirely to compression, with the thermodynamic state of the plasma regarded as virtually irrelevant until the evolution reaches advanced stages. The calculations presented here, however, suggest that the intrinsic component exerts a much more active, if unappreciated, influence in stream-interaction dynamics. In this view, intrinsic density-temperature-velocity correlations can substantially enhance the dynamic aspects of stream evolution and offset the kinematic steepening. The pressure gradients arising from the stream interaction drive nonradial flows which, though always small compared to the radial motion, allow the colliding material to slip laterally and spread the compression over a larger volume. Thus when the multi-dimensional dynamic reaction of the gas is considered, the compressive build-up of density and temperature at the leading edge of the stream is significantly reduced, and it follows that much of the density and temperature structure associated with streams is directly attributable to the intrinsic component. This entire topic, utilizing Helios observations will be treated at length in a subsequent paper.

The efficacy of the dynamical broadening mechanism as influenced by the intrinsic parameter correlations bears upon the question of whether a corotating shock will form. Inside 1 AU, the nonradial flow is readily induced and highly capable of dynamically relieving the stresses built up

in the stream interaction and thus acts to prevent shock formation. At large radial distances, however, the combination of low sound speed and more radial orientation of the stream-front gradients seriously inhibits the generation of nonradial flows. Therefore, shock formation is favored in those instances where the stream reaches large r while yet possessing enough excess momentum to continue that steepening. The amplitude, input parameter correlations, and longitudinal scale all affect the dynamic balance within a stream and jointly determine whether the evolution of a given structure will culminate in the formation of a corotating shock pair.

The implementation of the fully nonlinear 3-D model permits us for the first time to obtain reliable quantitative estimates of the meridional flow effects generated in the stream interaction. Our calculations suggest that even in the presence of substantial meridional gradients, the latitudinal transport of mass, energy, and momentum by streams appears to have little impact upon the overall evolution of the structure. In this regard, the meridional flow merely augments the action of the 2-D east-west flow in broadening and reducing stresses at the stream front. We cannot rule out the possibility that there may exist some extreme pathological stream configurations for which these findings will not hold true. Indeed, we expect some breakdowns in this behavior along the fringes of streams or in cases where the stream amplitude is low (trough-to-peak speed difference less than the sound speed). Nevertheless, across the main portion of a stream structure, where the velocity amplitude is high (and the radial kinetic momentum, therefore, large), we can be confident that the east-west rotational interaction dominates and that the north-south flow effects are necessarily small.

Since there is little latitudinal spreading of streams in interplanetary space, our 3-D solution at any given latitude across a stream does not differ appreciably from a 2-D solution executed for the equivalent longitudinal source conditions. It appears, then, that a viable 3-D model may be synthesized from a series of 2-D solutions at discrete latitudes, at some savings in computational effort. In addition, as more elaborate physical descriptions are introduced, there now exists explicit justification for developing these sophistications in a comparatively economical 2-D formulation.

It is to be emphasized that this result strictly applies only to corotating streams and not necessarily to transient flow structures, such as flare-related interplanetary shocks. It is true that the momentum arguments we have developed are sufficiently general to apply to such flows, and, in fact, elements of this view have previously been invoked in the analysis of the propagation of these structures (e.g., Hundhausen, 1973b). A crucial disparity is to be found, however, between the geometry of a corotating stream and that of a transient flow. Rotation induces a strong anisotropy into stream dynamics, such that the interaction is constrained to occur along a spiral front that lies nearly in an east-west plane. Thus fast and slow fluid elements experience a relatively oblique collision in which the tangential slippage normal to the plane of the interaction (i.e., the meridional motion) is only weakly driven. Transient flows, on the other hand, are not restricted to this favorable geometry, and there is no reason to expect that the induced meridional flows should be any less significant than the azimuthal flows. Given the enormous momenta associated with these events and the large gradients they produce in the interplanetary medium, it is therefore prudent to exercise some caution in extending the legitimacy of the 2-D approximation to models of transient flows.

While the 3-D flow effects covered in this paper have proven negligible in so far as stream evolution is concerned, it must not be construed that 3-D models are superfluous. Indeed, we have sketched out how the systematic flow variations at stream fronts can be exploited as a valuable probe of 3-D solar wind structure. Theoretical progress in this direction is explicitly dependent upon 3-D models, as are other provocative research topics. For example, angular momentum transport by streams appears small in the HD cases we have examined, but we could not rule out the possibility that significant effects might have been overlooked. By virtue of the fact that meridional and azimuthal speeds are of roughly the same order, estimates of the angular momentum flux (or any other parameter directly proportional to the azimuthal velocity) are particularly susceptible to modifications in the east-west flow induced by stream dynamics. In addition, our analysis of this effect is incomplete owing to the neglect of the magnetic field. Therefore, proper treatment of the angular momentum question and other implicitly global phenomena, such as the

Rosenberg-Coleman Effect (Coleman and Rosenberg, 1971) and the systematic north-south magnetic deflections associated with stream fronts (Rosenberg et al., 1978), await the application of 3-D MHD models.

[With regard to limitations imposed by neglect of the IMF, we stress that the main action of the field should be to augment the gas pressure forces and thus represents only a quantitative change in the dynamics. In the language of our previous exposition, the inclusion of the magnetic field must enhance the dynamic, as opposed to kinematic, attributes of the evolution. These effects should be most important where the gradients are largest, and it is for this very reason that we have avoided consideration of sharply-bounded structures like those reported by Helios. However, we do not anticipate that inclusion of the IMF will lead to any radical change in our stated conclusions, for the system remains strongly supersonic and superalfvenic.]

Though we may elect to dispense with a formal 3-D computation in some instances, we most emphatically may not dispense with a 3-D perspective. On the basis of Helios observations and inferences drawn from other spacecraft data, it has become accepted that sharp latitudinal variations in stream properties occur in the solar wind. Our calculations provide a firm theoretical background for this hypothesis. It has long been recognized that the presence of such sharply delineated structure severely compounds the interpretation of spacecraft data, which are garnered from precious few locations at any one time. In face of these inhospitable circumstances, efforts to deduce the latitudinal structure of the solar wind have been largely guided by the conviction that by accumulating massive amounts of data over a sufficiently great span of time or space (or both), it would be proper to relate various average quantities to meridional or radial gradients or other characteristic properties predicted by smooth-flow axisymmetric models. It has recently been demonstrated that such procedures are fraught with dangers, even when such simple properties as radial flow variations are assayed (Hundhausen, 1978). We would only add that the adversities of the situation are compounded if one seeks support or condemnation of theoretical prognostications in more subtle parameters--such as average nonradial flows--severely affected by stream dynamics and intimately related to the local structure.

In summation, if we hope to learn any significant new solar wind physics, our analyses must be attuned to the undeniable structured nature of the medium and a keen awareness of the 3-D aspects of the flow must permeate our thinking. Some studies have already incorporated this philosophy to varying degrees, and we can only be encouraged that further application of these methods to the vast stores of data now available from IMP, Helios, Pioneer, and Voyager, to name a few, will inevitably lead to great advances in our understanding of the global solar wind flow.

ACKNOWLEDGMENTS

This work was initiated while the author was a graduate assistant at the High Altitude Observatory of the National Center for Atmospheric Research (The National Center for Atmospheric Research is funded by the National Science Foundation) and was completed while he was an NAS/NRC Resident Research Associate at NASA/Goddard Space Flight Center. He wishes to thank Drs. A. J. Hundhausen, T. E. Holzer, R. G. Athay, J. M. Malville, S. T. Suess, J. T. Gosling, J. Feynmman and G. Newkirk, Jr., for their encouragement during the early phases of this research, and Drs. L. F. Burlaga, J. D. Scudder, K. W. Ogilvie, and N. F. Ness for their support, advice, and hospitality during the author's stay at Goddard.

Some of the illustrations for this paper were generated with portable versions of NCAR graphics routines, which are freely supplied by that institution.

REFERENCES

Bame, S. J., J. R. Asbridge, W. C. Feldman, and J. T. Gosling, Evidence for a structure-free state at high solar wind speeds, J. Geophys. Res., 82, 1487, 1977.

Barouch, E., Properties of the solar wind at 0.3 AU inferred from measurements at 1 AU, J. Geophys. Res., 82, 1493, 1977.

Barouch, E. and L. F. Burlaga, Three-dimensional interplanetary stream magnetism and energetic particle motion, J. Geophys. Res., 81, 2103, 1976.

Bohlin, J. D. and D. M. Rubenstein, Synoptic maps of solar coronal hole boundaries derived from He II 304 Å spectoheliograms from the manned Skylab missions, Rep. UAG-51, World Data Center A, NOAA, Boulder, CO, 1975.

Burlaga, L. F., Interplanetary stream interfaces, J. Geophys. Res., 79, 3717, 1974.

Burlaga, L. F. and K. W. Ogilvie, Magnetic and thermal pressures in the solar wind, Solar Phys., 15, 61, 1970.

Burlaga, L. F. and K. W. Ogilvie, Solar wind temperature and speed, J. Geophys. Res., 78, 2028, 1973.

Burlaga, L. F., K. W. Ogilvie, D. H. Fairfield, M. D. Montgomery, and S. J. Bame, Energy transfer at colliding streams in the solar wind, Astrophys. J., 164, 137, 1971.

Carovillano, R. L. and G. L. Siscoe, Corotating Structure in the solar wind, Solar Phys., 8, 401, 1969.

Coleman, P. J., Jr. and R. Rosenberg, North-south component of the interplanetary magnetic field, J. Geophys. Res., 76, 2917, 1971.

Dryer, M. and R. S. Steinolfson, MHD solution of interplanetary disturbances generated by simulated velocity perturbations, J. Geophys. Res., 81, 5413, 1976.

Feldman, W. C., J. R. Asbridge, S. J. Bame, and J. T. Gosling, High-speed solar wind flow parameters at 1 AU, J. Geophys. Res., 81, 5054, 1976.

Goldstein, B. E., Nonlinear corotating solar wind structure, Rep. CSR-P-71-63, Mass. Inst. of Tech., Cambridge, 1971.

Goldstein, B. E. and J. R. Jokipii, Effects of stream-associated fluctuations upon the radial evolution of average solar wind flow parameters, J. Geophys. Res., 82, 1095, 1977.

Gosling, J. T., A. J. Hundhausen, V. Pizzo, and J. R. Asbridge, Compressions and rarefactions in the solar wind: Vela 3, J. Geophys. Res., 77, 5442, 1972.

Gosling, J. T. J. R. Asbridge, S. J. Bame, and W. C. Feldman, Solar wind stream interfaces, J. Geophys. Res., 83, 1401, 1978.

Han, S. M., A numerical study of two-dimensional time-dependent magnetohydrodynamic flows, Ph. D. Thesis, University of Alabama in Huntsville, 1977.

Hewish, A., Observations of the solar plasma using radio scattering and scintillation methods, Solar Wind, NASA/SP 308, 477, 1972.

Hundhausen, A. J., Nonlinear model of high-speed solar wind streams, J. Geophys. Res., 78, 1528, 1973a.

Hundhausen, A. J., Evolution of large-scale solar wind structures beyond 1 AU, J. Geophys. Res., 78, 2035, 1973b.

Hundhausen, A. J., An interplanetary view of coronal holes, in A Monograph on Coronal Holes, edited by J. B. Zirker, chap. 7, University of Colorado, Boulder, 1977.

Hundhausen, A. J., Solar wind spatial structure: the meaning of latitude gradients in observations averaged over solar longitude, J. Geophys. Res., 83, 4186, 1978.

Hundhausen, A. J. and L. F. Burlaga, A model for the origin of solar wind stream interfaces, J. Geophys. Res., 80, 1845, 1975.

Lazarus, A. J. and B. E. Goldstein, Observation of the angular momentum flux carried by the solar wind, Astrophys. J., 168, 571, 1971.

MacCormack, R. W., Numerical solution of the interaction of a shock wave with a laminar boundary layer, in Proceedings of the Second International Conference on Numerical Methods in Fluid Dynamics, Lecture Notes in Physics, vol. 8, edited by M. Holt, p. 151, Springer, New York, 1971.

Matsuda, T. and T. Sakurai, Dynamics of the azimuthally-dependent solar wind, Cosmic Electrodynamics, 3, 97, 1972.

Nakagawa, Y. and R. E. Wellck, Numerical studies of azimuthal modulations of the solar wind with magnetic fields, Solar Phys., 32, 257, 1973.

Nerney, S. F. and S. T. Suess, Restricted three-dimensional stellar wind modeling, Astrophys. J., 196, 837, 1975.

Neugebauer, M., The quiet solar wind, J. Geophys. Res., 81, 4664, 1976.

Pizzo, V., A three-dimensional model of corotating streams in the solar wind 1. Theoretical foundations, J. Geophys. Res., 83, 5563, 1978.

Pizzo, V., A three-dimensinal model of corotating streams in the solar wind III. Magnetohydrodynamic streams (in preparation), 1979.

Pizzo, V., J. T. Gosling, A. J. Hundhausen, and S. J. Bame, Large-scale dynamical effects upon the solar wind flow parameters, J. Geophys. Res., 1978, 6469, 1973.

Riesebieter, W., Dreidimensionale Modelbrechnungen zum Solaren Wind, Ph. D. Thesis, Technischen Universitat zu Braunschweig, FRG, 1977.

Rosenbauer, H., R. Schwenn, E. Marsch, B. Meyer, H. Miggenrieder, M. D. Montgomery, K. H. Muhlhauser, W. Pilipp, W. Voges, and S. M. Zink, A survey of initial results of the Helios plasma experiment, J. Geophys., 42, 561, 1977.

Rosenberg, R. and P. J. Coleman, Jr., Solar-cycle dependent north-south field configurations observed in solar wind interaction regions, Pub. No. 1804, Inst. of Geophysics and Planetary Physics, UCLA, 1978.

Siscoe, G. L. Structure and orientations of solar wind interaction fronts: Pioneer 6, J. Geophys. Res., 77, 27, 1972.

Siscoe, G. L. and L. T. Finley, Solar wind structure determined by corotating coronal inhomogeneities, 2, Arbitrary perturbations, J. Geophys. Res., 77, 35, 1972.

Winge, C. W. and P. J. Coleman, Jr., First-order latitude effects in the solar wind, Planetary and space Sci., 22, 439, 1972.

Woo, R., Multifrequency techniques for studying interplanetary scintillations, Astrophys. J., 201, 238, 1975.

Zirker, J. B., Coronal holes and high-speed wind streams, Rev. of Geophys. and Space Phys., 15, 257, 1977.

FIGURE CAPTIONS

FIGURE 1 — Contours of constant radial velocity, u_r, for the prototype stream projected on the source surface r_o = 0.16 AU = 35 R_S. The speed is indicated in km/s and Δ refers to the contour increment. North is at top, west to the right. The slight irregularities in the contours are caused by minor inadequacies in the contouring routine.

FIGURE 2 — Contours of constant (a) radial velocity, (b) number density, (c) temperature, and (d) pressure for the prototype stream at 1.0 AU. Highs and lows for each parameter are marked by the "H" and "L", and Δ indicates the contour increment in each case.

FIGURE 3 — The nonradial flow induced by the prototype stream at 1.0 AU. The length and orientation of the vectors show the magnitude and direction of the local flow on the surface of the 1.0 AU sphere. The large arrow at bottom indicates the minimum radial velocity, to emphasize the small value of the nonradial deflections. There is a general transport of mass, energy, and momentum away from the compression and into the rarefaction.

FIGURE 4 — The top panel shows the net latitudinal transport of mass, M, energy, E, and radial momentum, D that is occasioned by the nonradial flows driven by the prototype stream between $35R_S$ and 1.0 AU. Positive values indicate flux gain, negative values, flux loss. The middle panel displays the average azimuthal momentum flux density, L_ϕ, and meridional momentum flux density, L_θ, induced by the stream evolution. Positive L_ϕ is associated with momentum in the direction of solar rotation, positive L_θ indicates north-to-south transport. The bottom panel shows a vertical slice through the center of the radial velocity distribution in Figure 1. All these curves are symmetric about the equator ($\theta = 90^\circ$).

FIGURE 5 Simulated spacecraft data taken along solar equator at 1.0 AU for three streams with different intrinsic parameter correlations, X, as defined in the text. From the top are plotted the radial velocity, number density, temperature, gas pressure, azimuthal velocity, and inertial frame flow angle as a function of angular position. Positive flow angle means in the direction of solar rotation (flow coming from the east). Azimuth, ϕ, converts to temporal units at the synodic rate of 13.3°/day.

FIGURE 6 Schematic of contour patterns at r_o for streams of total longitudinal breadth = 30°, 60°, and 120°. The meridional breadth is constant at 60°.

FIGURE 7 Schematic of contour patterns at r_o for streams of total meridional breadth = 30°, 60°, and 120°. The longitudinal breadth is constant at 60°.

FIGURE 8 The dependence of stream evolution upon source latitude. The top panel shows the radial velocity contours for otherwise identical streams centered at the equator, at $+45^{\circ}$N, and at the north pole. The bottom two panels show the resultant contours at 1.0 AU for radial velocity and pressure. Note the change of scales for the pressure plot of the polar stream.

FIGURE 9 Radial velocity contours at $r_o = 35\ R_S$ for the asymmetric stream. The intrinsic parameter correlations of equation (8) are in effect, so the density and temperature contours mimic those pictured for u_r.

FIGURE 10 Radial velocity, density, temperature, and pressure contours for the asymmetric stream at 1.0 AU. The interaction has taken place diagonally to the equator.

FIGURE 11 The nonradial flow associated with the asymmetric stream at 1.0 AU, projected on the pressure contours of Figure 10d.

FIGURE 12 The relative displacement of tracer particles embedded in the asymmetric stream between 35 R_S and 1.0 AU. The particles were arrayed on the source surface in a uniform 5^o x 5^o grid. Most of the east-west displacement is due to rotational re-alignment of fluid moving with different radial velocities, and the remainder is attributable to deflections acquired in the subsequent interaction.

FIGURE 13 Latitudinal flux transport in the asymmetric stream as a function of colatitude, θ. Despite the huge gradients in all parameters, the net transport of mass, energy and momentum due to the stream interaction remains small.

FIGURE 14 Comparison of 3-D and 2-D solutions along equator of asymmetric stream at 1.0 AU. The latitudinal gradients have had little effect upon the local evolution.

FIGURE 15 The two basic kinds of nonradial flow resulting from pressure forces associated with the stream interaction. In pure edge flow, (a), the meridional motions arise strictly from latitudinal gradients along the pressure ridge and are out of phase with the azimuthal flow. In direct-driven flow, (b), the meridional motions are propelled by the inclination of the pressure gradients to the equator and are in phase with the azimuthal flow. In general, observed motions will be a combination of the two classes.

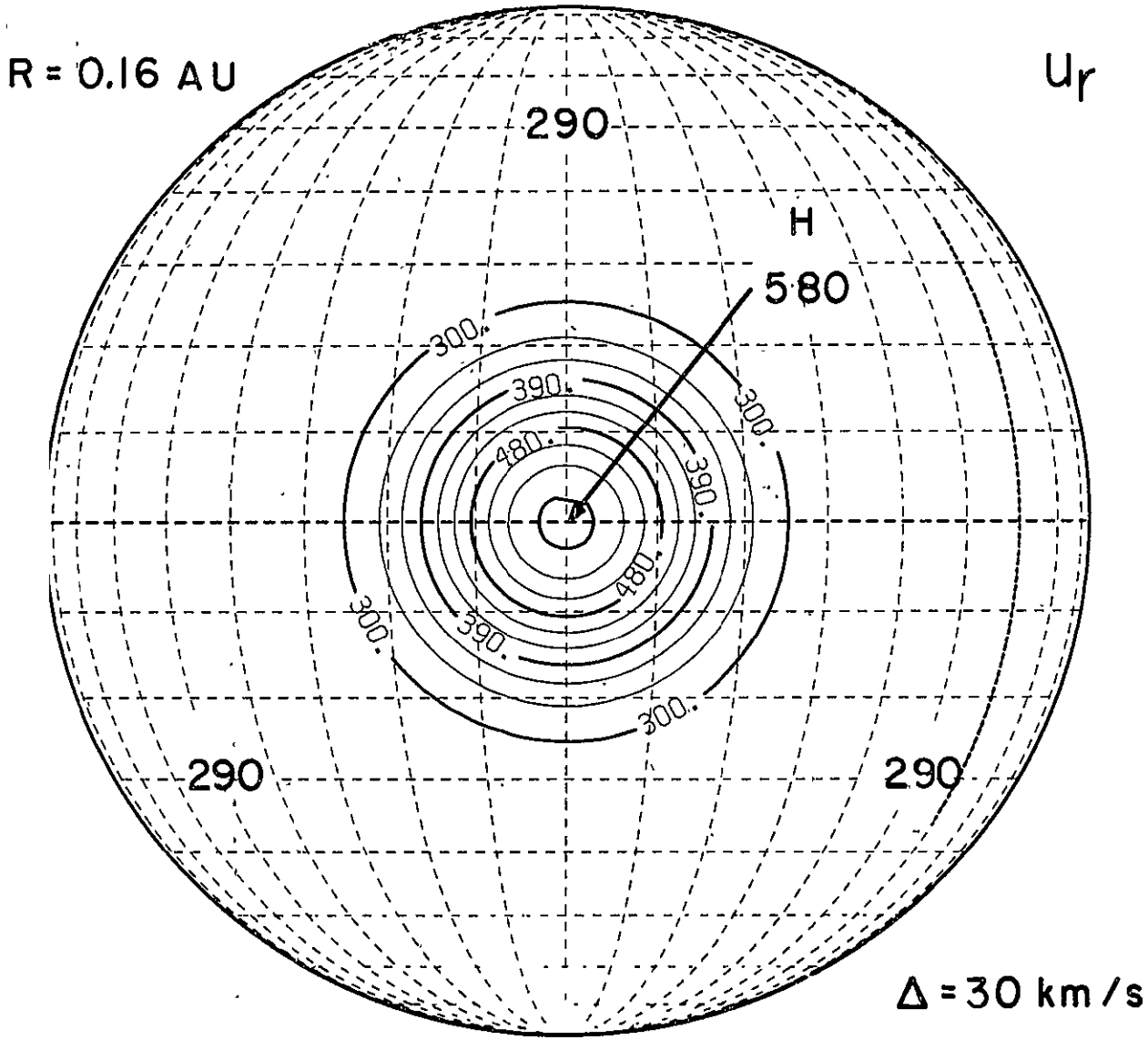
R = 0.16 AU
U_r
290
H
580
300.
390.
480.
300.
390.
480.
300.
390.
300.
290
290
Δ = 30 km/s

Figure 1

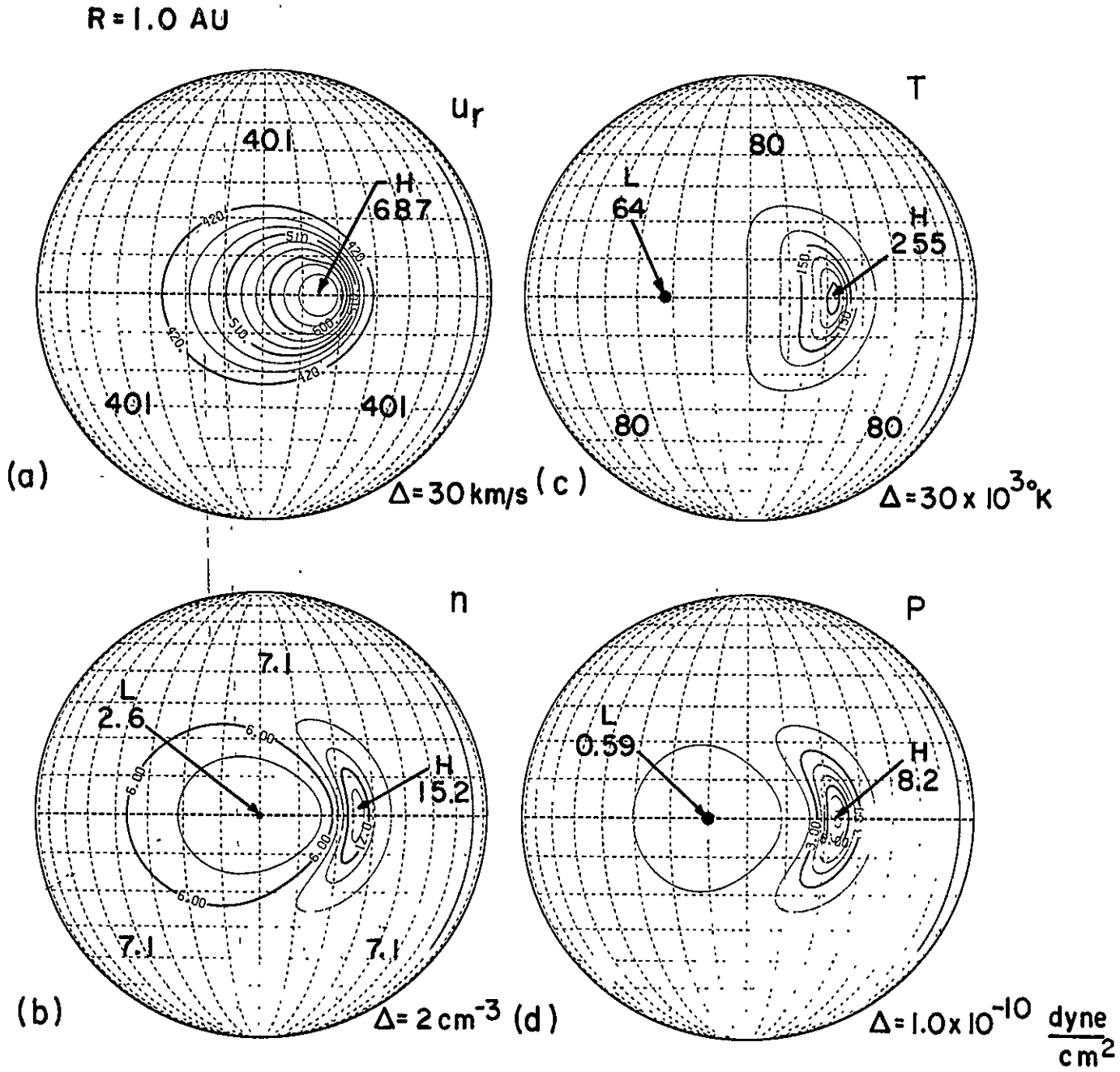
R = 1.0 AU
u_r
401
H
687
420
510
600
420
510
420
401
401
(a)
Δ = 30 km/s
T
80
L
64
H
255
150
80
80
(c)
Δ = 30 x 10^3 °K
n
7.1
L
2.6
6.00
6.00
6.00
6.00
H
15.2
7.1
7.1
(b)
Δ = 2 cm^{-3}
P
L
0.59
H
8.2
3.00
(d)
Δ = 1.0 x 10^{-10} $\frac{dyne}{cm^2}$

Figure 2

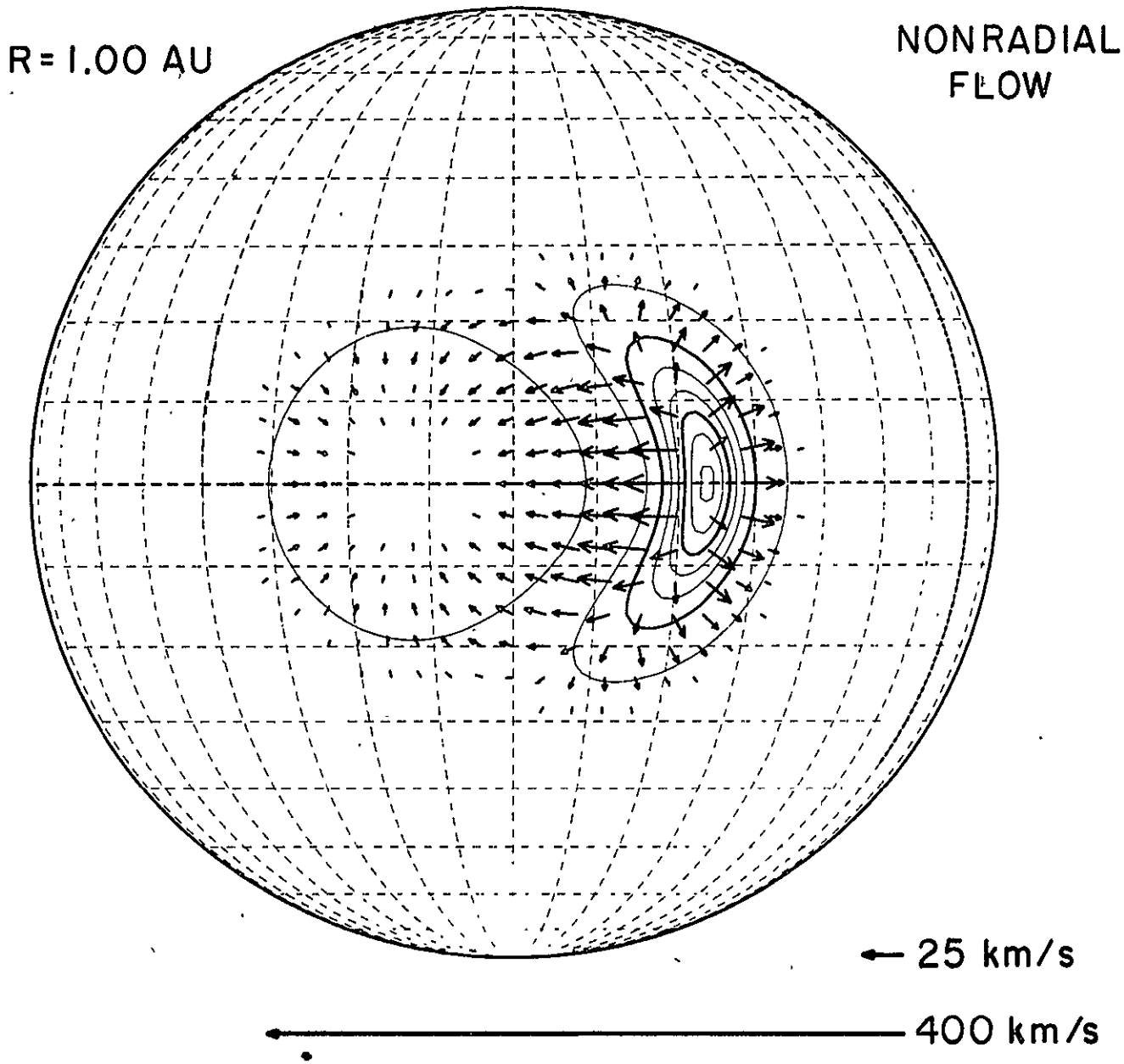

Figure 3

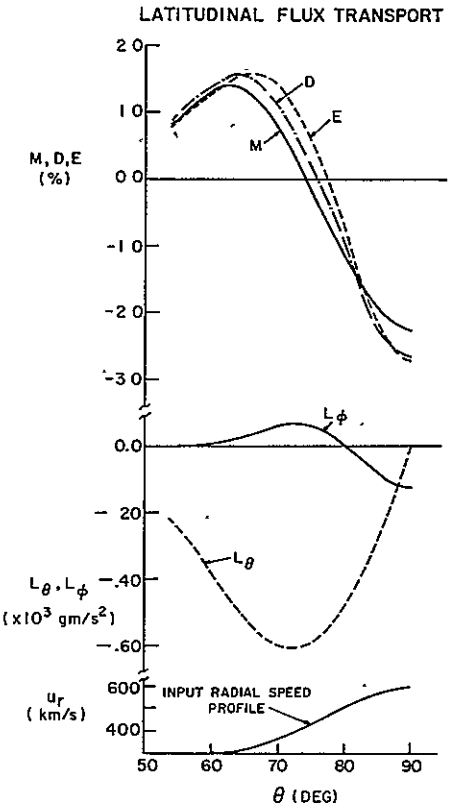
LATITUDINAL FLUX TRANSPORT
M, D, E (%)
2 0
1 0
0 0
-1 0
-2 0
-3 0
D
E
M
L_ϕ
0.0
- 20
L_θ
L_θ, L_ϕ ($\times 10^3$ gm/s^2)
-.40
-.60
u_r (km/s)
600
400
INPUT RADIAL SPEED PROFILE
50
60
70
80
90
θ (DEG)

Figure 4

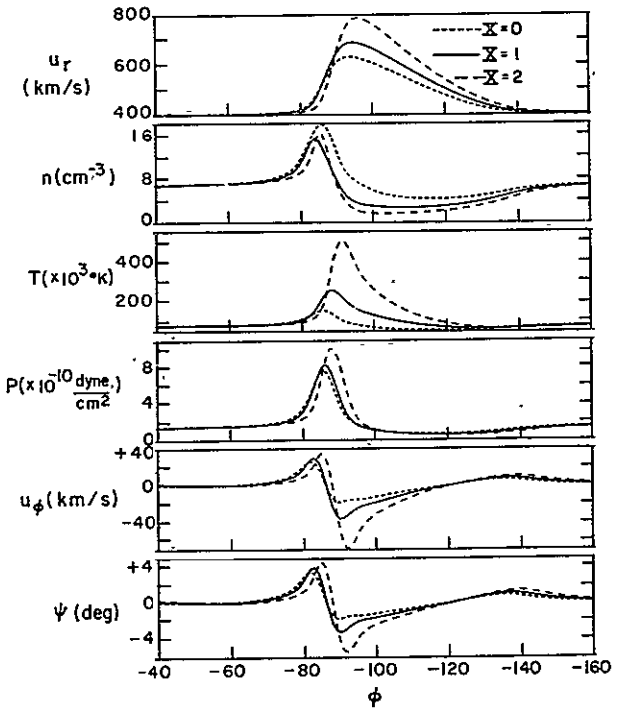
800
600
400
u_r (km/s)
X=0
X=1
X=2
16
8
0
n(cm^{-3})
400
200
T(x10^3°K)
8
4
0
P(x10^{-10} dyne/cm^2)
+40
0
-40
u_ϕ(km/s)
+4
0
-4
ψ (deg)
-40
-60
-80
-100
-120
-140
-160
φ

Figure 5

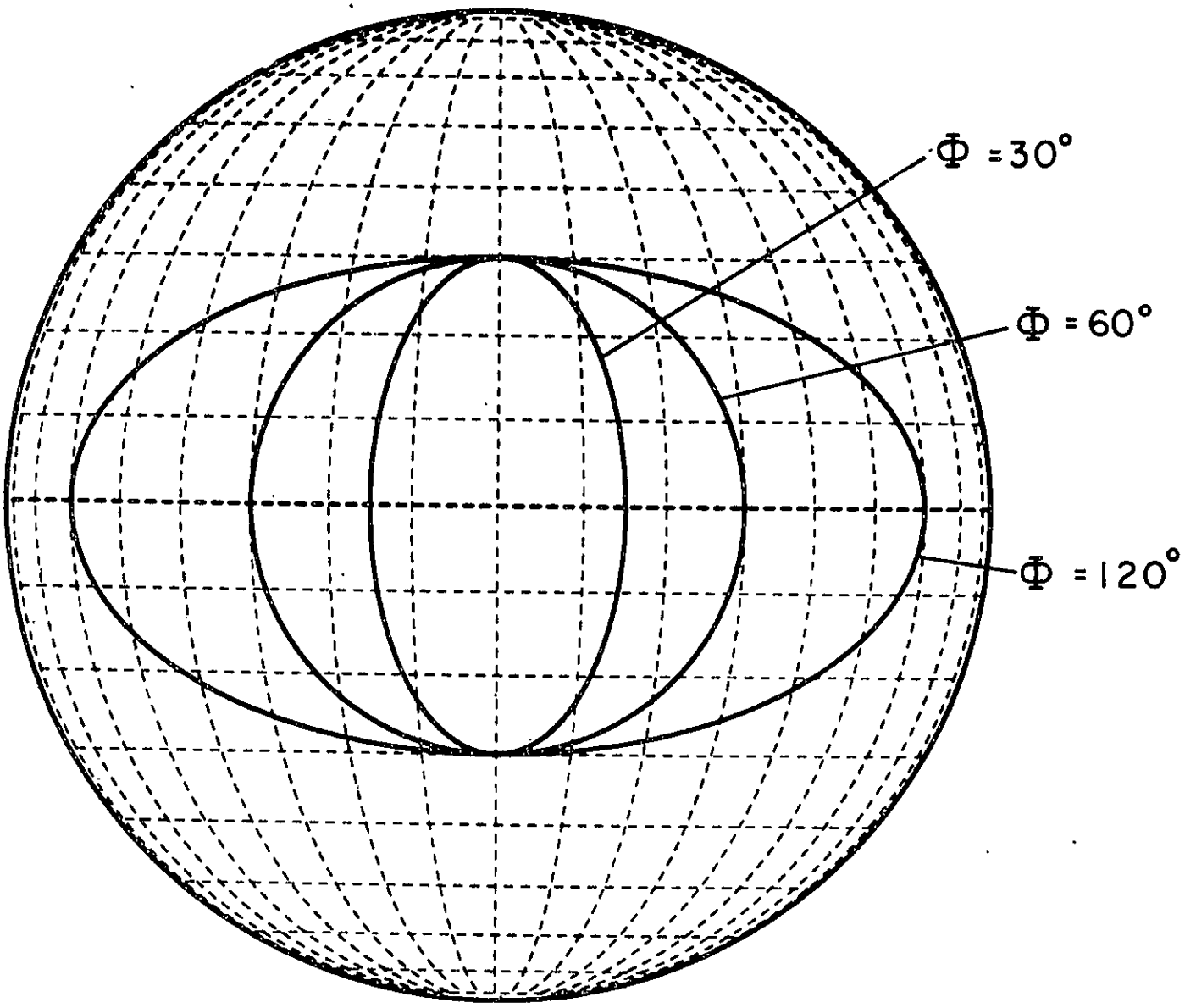

Figure 6

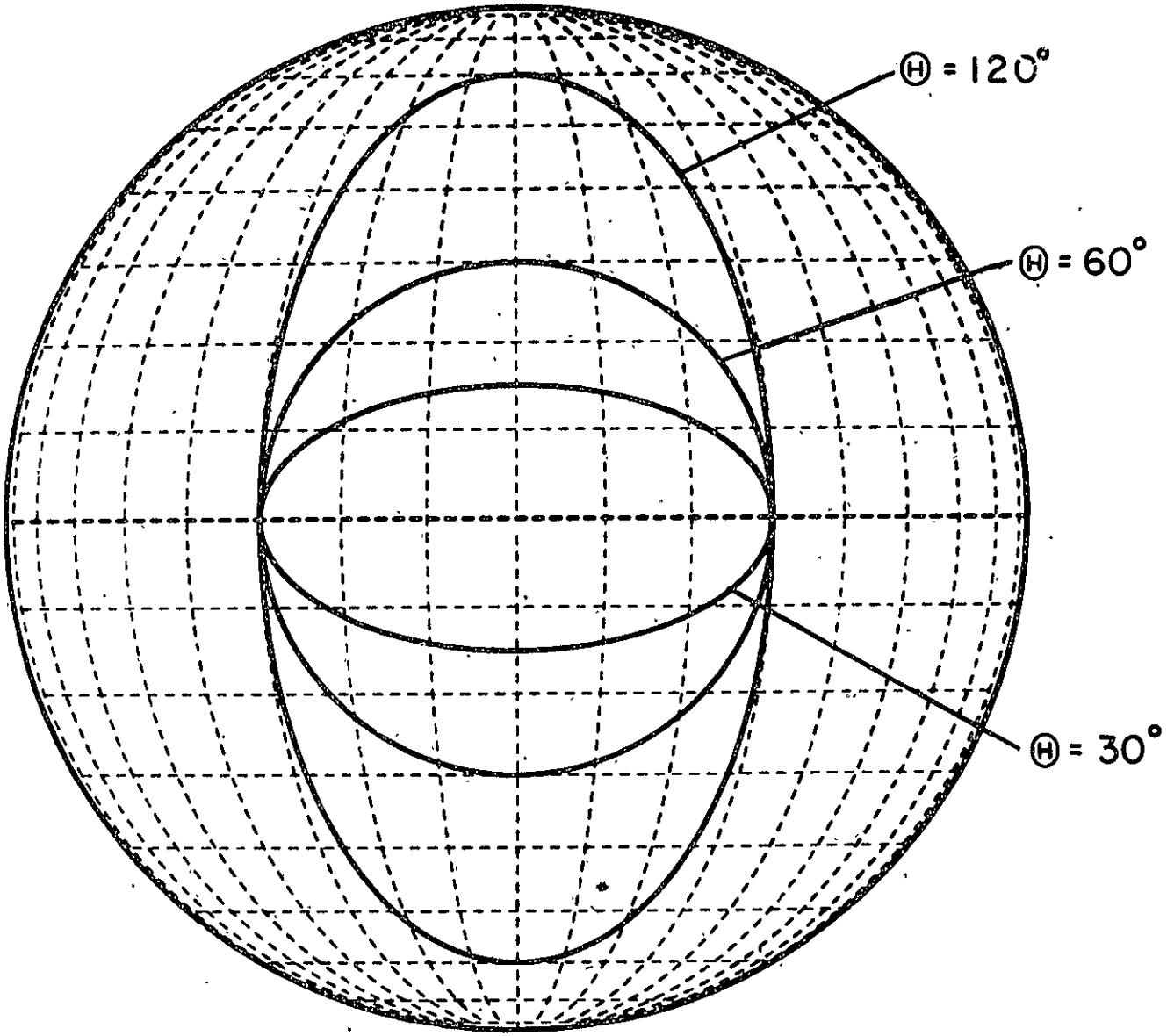

Figure 7

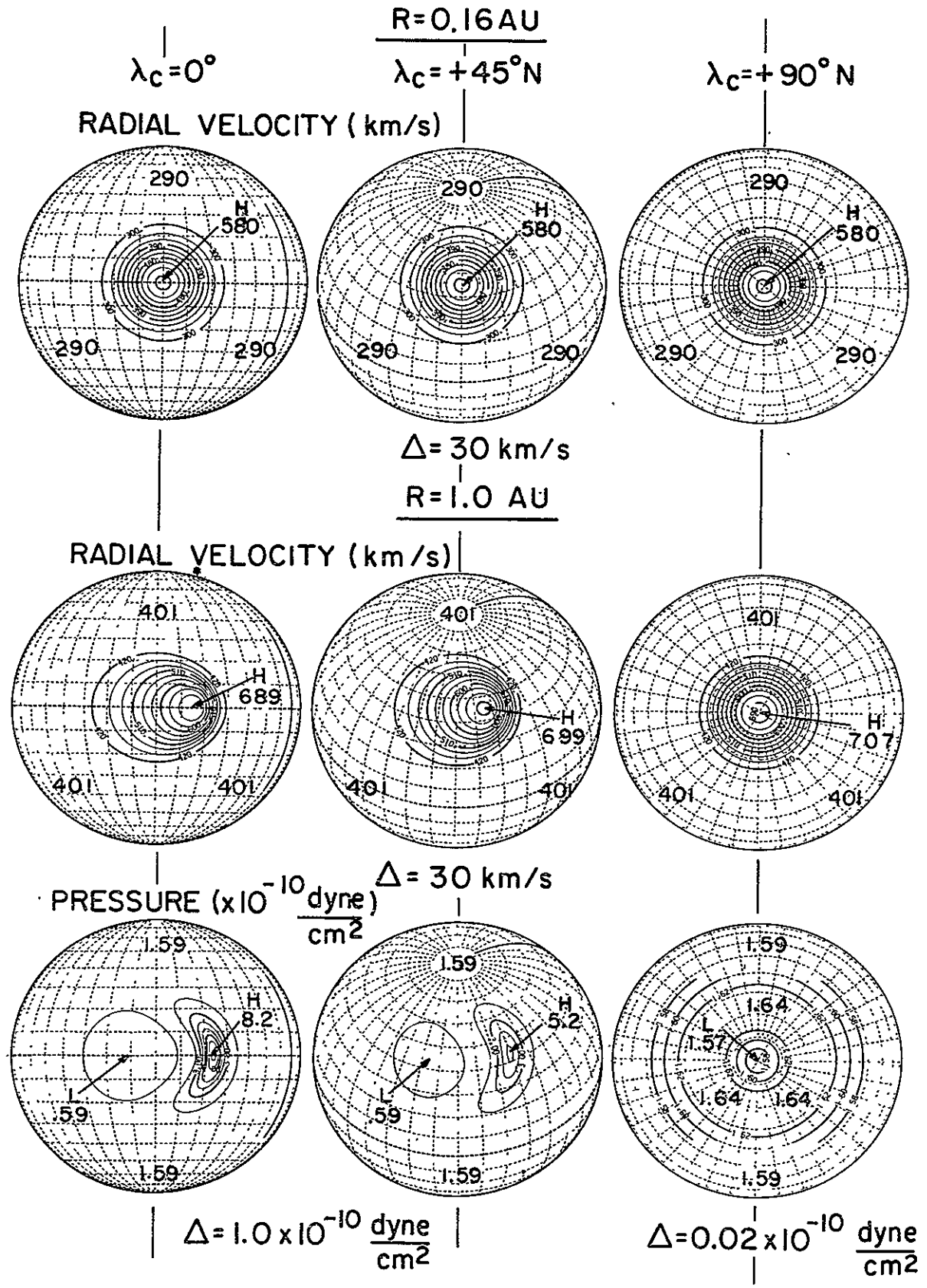
R=0.16 AU
λc=0°
λc=+45°N
λc=+90°N
RADIAL VELOCITY (km/s)
290
H
580
290
290
Δ=30 km/s
R=1.0 AU
RADIAL VELOCITY (km/s)
401
H
689
699
707
401
401
Δ=30 km/s
PRESSURE (x10^-10 dyne/cm^2)
1.59
H
8.2
5.2
L
.59
1.64
1.57
Δ=1.0 x 10^-10 dyne/cm^2
Δ=0.02 x 10^-10 dyne/cm^2

Figure 8

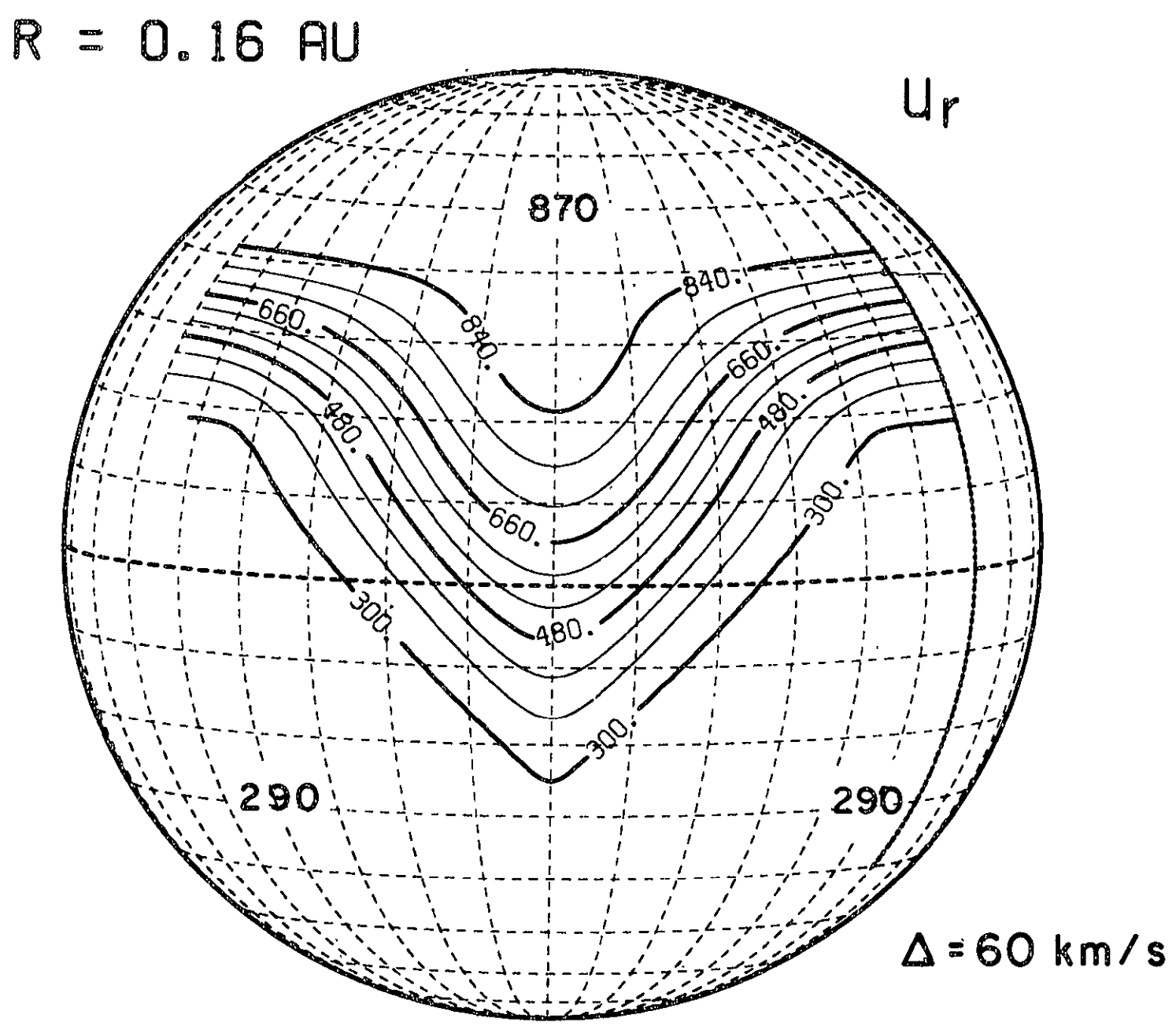

Figure 9

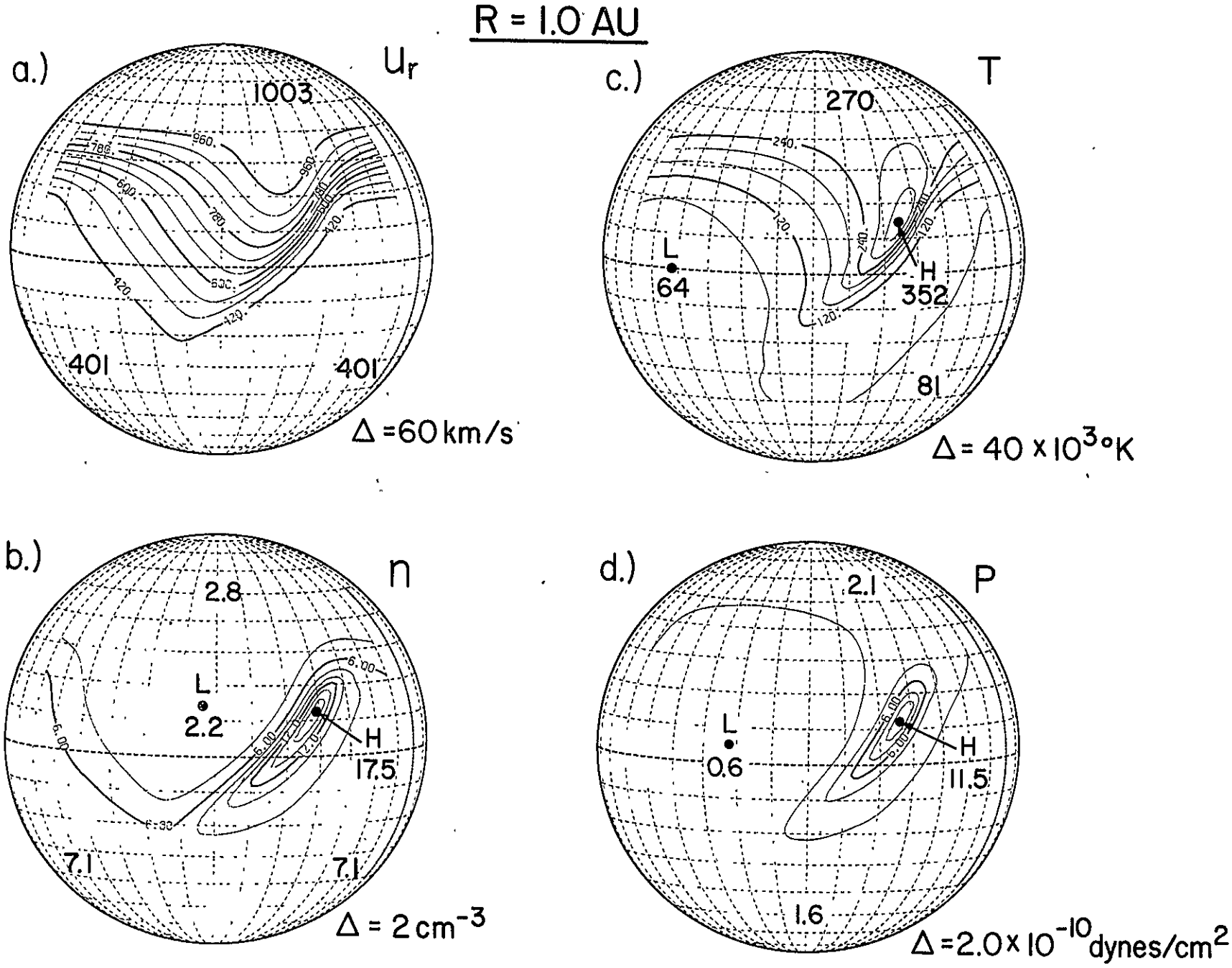
R = 1.0 AU
a.)
U_r
1003
960.
780.
600.
420.
540.
120.
401
401
Δ =60 km/s
c.)
T
270
240.
120.
L
64
H
352
81
Δ = 40 x 10³ °K
b.)
n
2.8
L
2.2
H
17.5
6.00
7.1
7.1
Δ = 2 cm⁻³
d.)
P
2.1
L
0.6
H
11.5
1.6
Δ =2.0 x 10⁻¹⁰ dynes/cm²

Figure 10

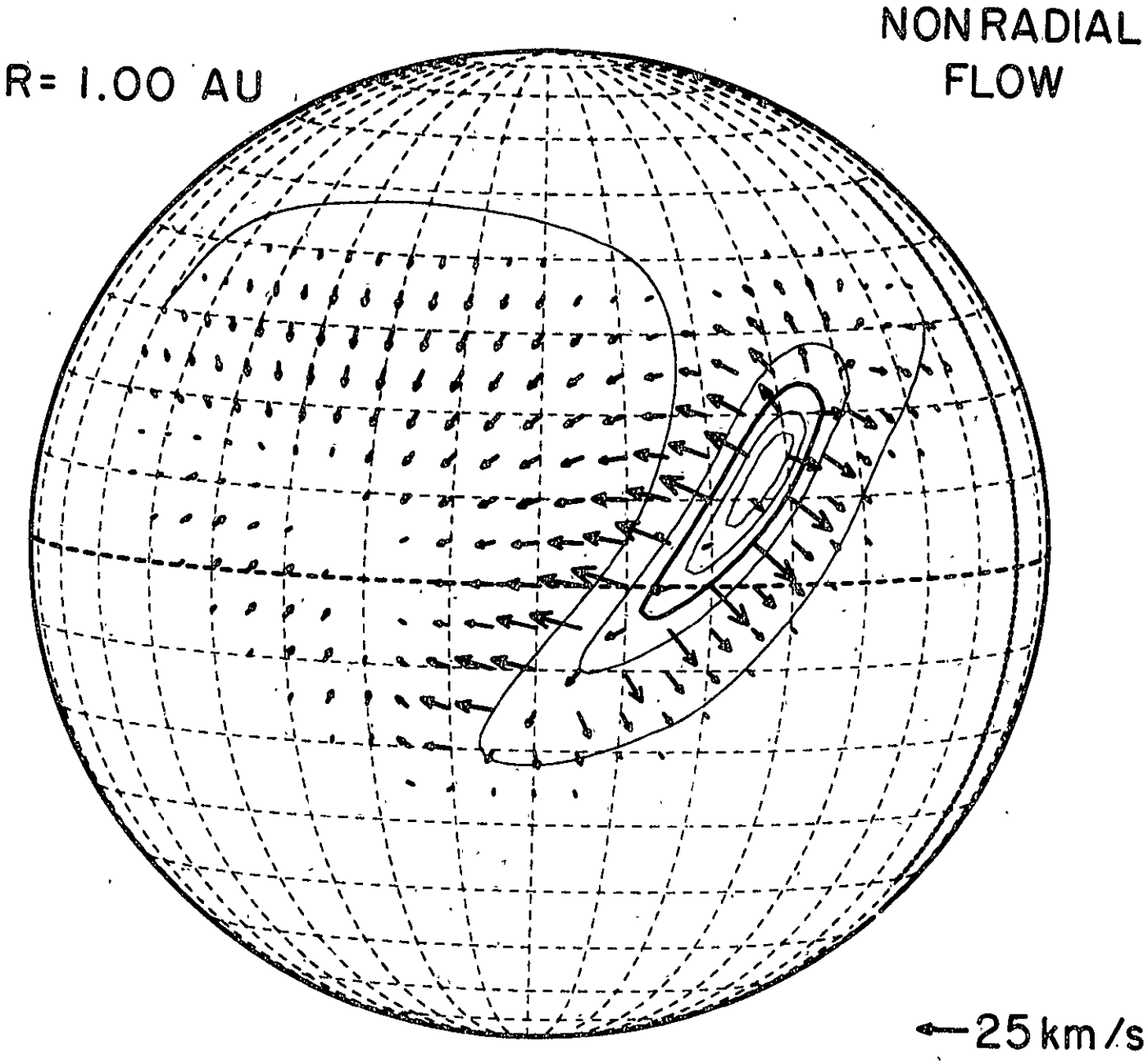

Figure 11

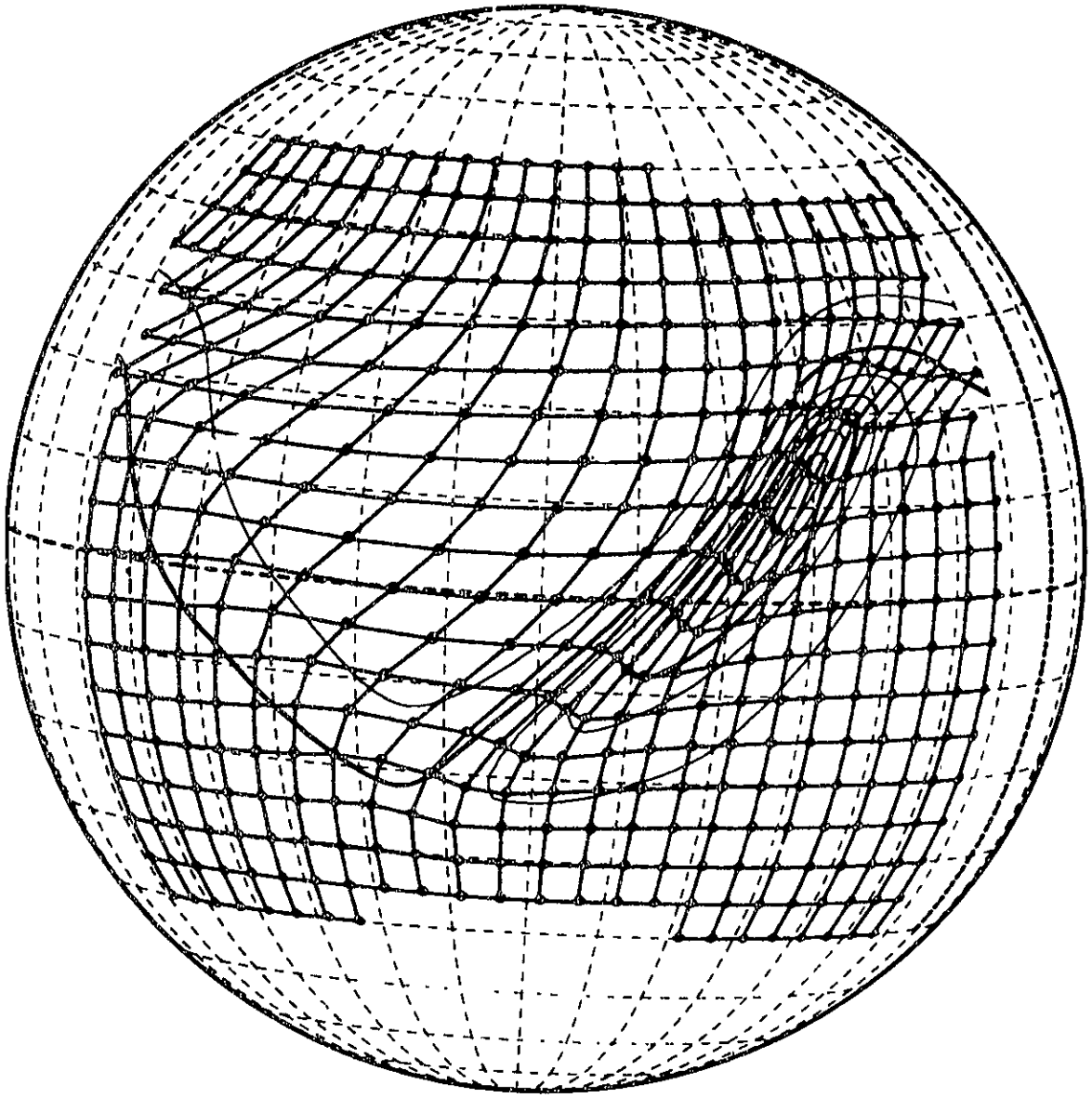

Figure 12

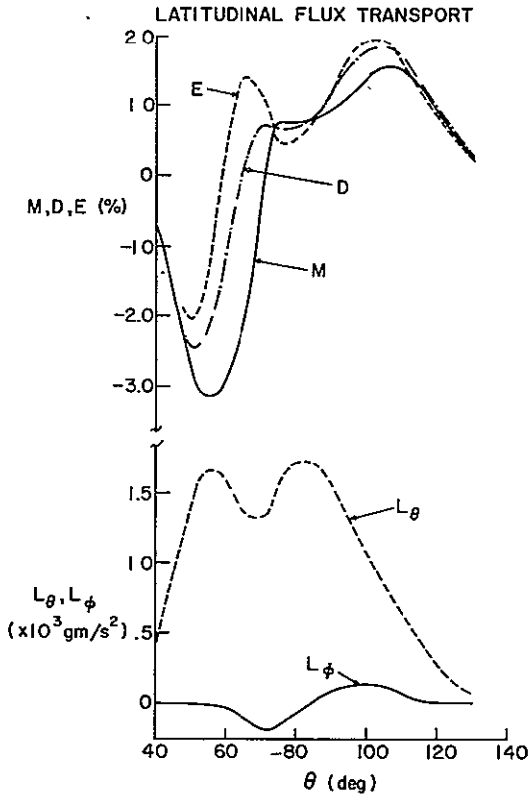
LATITUDINAL FLUX TRANSPORT
2.0
1.0
0
-1.0
-2.0
-3.0
M,D,E (%)
E
D
M
1.5
1.0
.5
0
L_θ, L_ϕ
($\times 10^3$ gm/s^2)
L_θ
L_ϕ
40
60
-80
100
120
140
θ (deg)

Figure 13

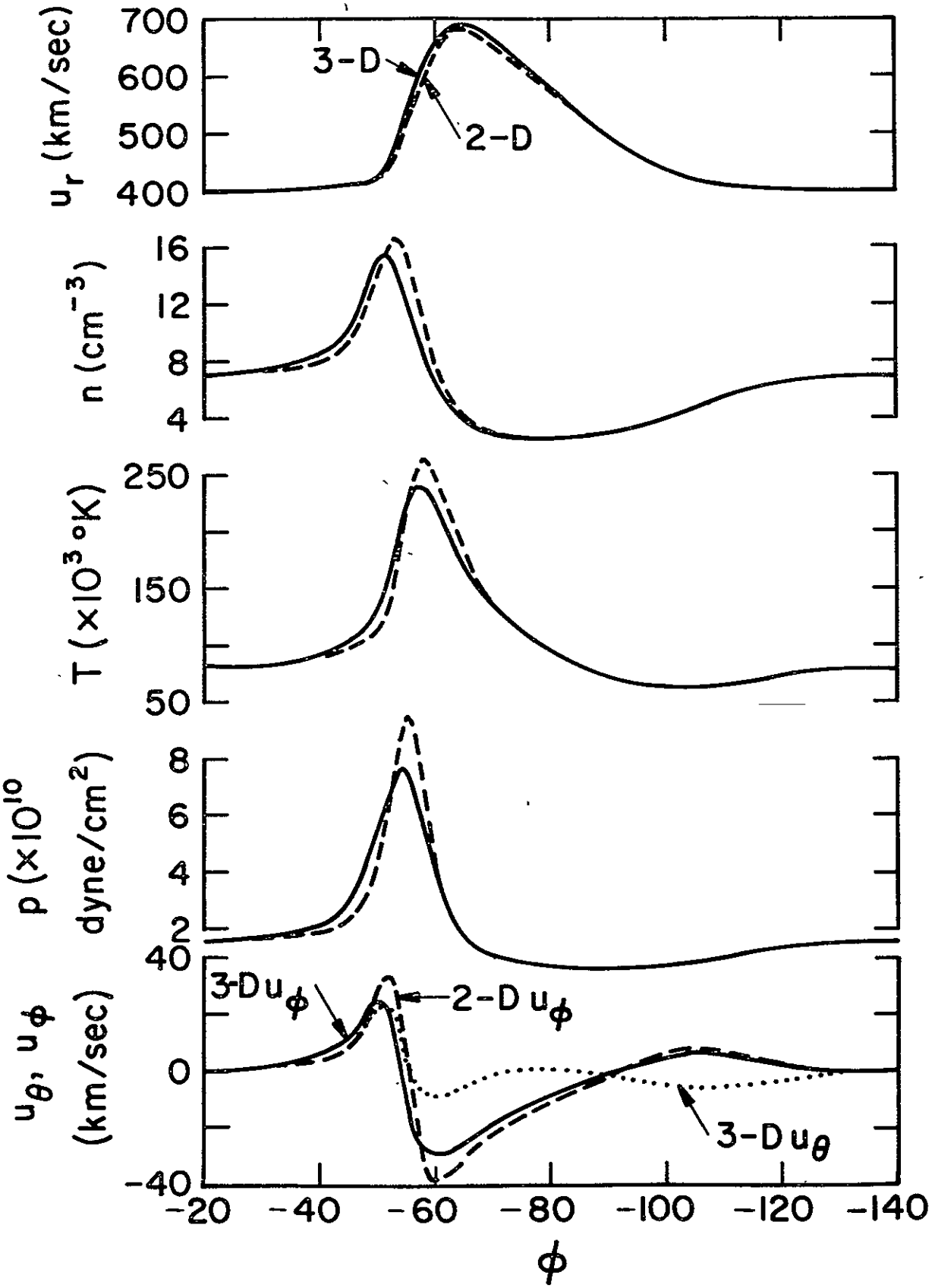
u_r (km/sec)
700
600
500
400
3-D
2-D
n (cm^{-3})
16
12
8
4
T ($\times 10^3$ °K)
250
150
50
p ($\times 10^{10}$ dyne/cm^2)
8
6
4
2
u_θ, u_ϕ (km/sec)
40
0
-40
3-D u_ϕ
2-D u_ϕ
3-D u_θ
-20
-40
-60
-80
-100
-120
-140
ϕ

Figure 14

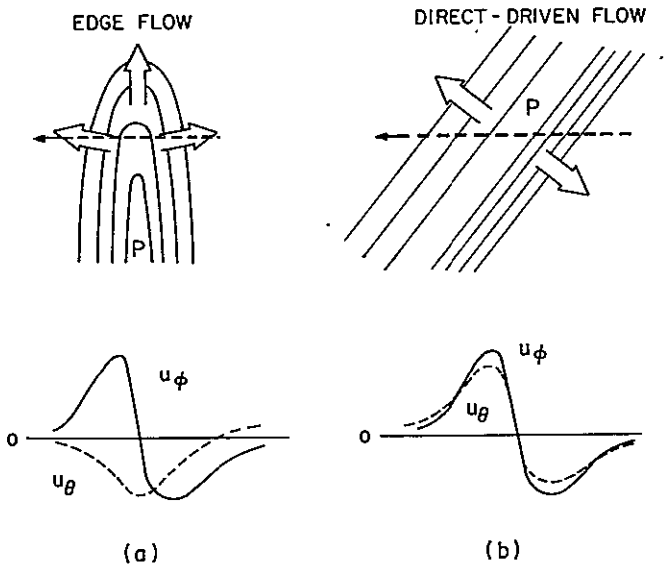
EDGE FLOW
DIRECT - DRIVEN FLOW
P
P
u_ϕ
u_θ
0
u_ϕ
u_θ
0
(a)
(b)

Figure 15

BIBLIOGRAPHIC DATA SHEET

1. Report No.	2. Government Accession No.	3. Recipient's Catalog No.
TM 80276		

4. Title and Subtitle	5. Report Date
A Three-Dimensional Model of Corotating Streams in the Solar Wind II. Hydrodynamic Streams	April 1979
	6. Performing Organization Code

7. Author(s)	8. Performing Organization Report No.
Victor J. Pizzo	

9. Performing Organization Name and Address	10. Work Unit No.
NASA/GSFC Laboratory for Extraterrestrial Physics Interplanetary Physics Branch, Code 692 Greenbelt, MD 20771	11. Contract or Grant No.
	13. Type of Report and Period Covered
12. Sponsoring Agency Name and Address	Technical Memorandum
	14. Sponsoring Agency Code

15. Supplementary Notes

16. Abstract

SEE ATTACHED.

17. Key Words (Selected by Author(s))	18. Distribution Statement
Solar wind streams	

19. Security Classif. (of this report)	20. Security Classif. (of this page)	21. No. of Pages	22. Price*
U	U	67	

*For sale by the National Technical Information Service, Springfield, Virginia, 22151.

ABSTRACT

This paper explores theoretical aspects of corotating solar wind dynamics on a global scale by means of numerical simulations executed with a nonlinear, inviscid, adiabatic, single-fluid, three-dimensional (3-D) hydrodynamic formulation. The study begins with a simple, hypothetical 3-D stream structure defined on a source surface located at 35 R_S and carefully documents its evolution to 1 AU under the influence of solar rotation. By manipulating the structure of this prototype configuration at the source surface, it is possible to elucidate the factors most strongly affecting stream evolution: 1) the intrinsic correlations among density, temperature, and velocity existing near the source; 2) the amplitude of the stream; 3) the longitudinal breadth of the stream; 4) the latitudinal breadth of the stream; and 5) the heliographic latitude of the centroid of the stream. The action of these factors is best understood in terms of momentum arguments of relative simplicity and general application (to the extent that waves, conduction, and kinetic effects may be ignored). Corotating structure is viewed as a spiral standing wave (in the rotating frame) in which there is an ongoing competition between the kinematic tendency of the stream to steepen (as high-speed material overtakes slow) and the dynamical reaction of the gas to resist compression (through acceleration and tangential deflection of material by pressure gradients in the interaction region). Longitudinal gradients in the radial velocity distribution determine how fast material is brought into the interaction region, but the detailed momentum balance as a function of position within the stream dictates what happens when the material collides. Reasonable specifications of the five factors mentioned above can so affect this kinematic-dynamic balance that even a high-amplitude stream (e.g., peak-to-trough velocity differences at 1 AU $\cong$ 480 km/s) may be prevented from shocking inside 1 AU, where the nonradial-flow broadening mechanism operates most efficiently. The nonlinear 3-D capabilities of the model allow quantitative study of the global development of this induced tangential flow in some detail. The nonradial motions lead to the net latitudinal transport of small amounts (a few percent) of mass, energy, and momentum. The effects of the latitudinal transport upon the evolution

within an east-west plane are minimal, and the latitudinal spreading of stream material in interplanetary space, even in the presence of steep meridional gradients (up to 30 km/s/deg), is limited to a few degrees. Thus, for corotating structures, with their favorable spiral geometry, the 2-D approximation adequately describes the dynamical interaction. However, certain important research topics can only be approached in the full 3-D formulation. For example, the systematic pattern of the meridional flow changes across stream fronts contain information on the 3-D structure of the stream and thus offers promise as a practical diagnostic tool. Also, since the magnetic field is tied to the flow, it is to be expected that stream-driven meridional motions should have a noticeable effect upon the north-south magnetic fluctuations and may be of consequence to angular momentum studies. Proper discussion of these subjects demands a 3-D MHD model and will be considered in a subsequent paper.